46. Buerkle MA, Pahernik SA, Sutter A, Jonczyk A, Messmer K, Dellian M. Inhibition of the alpha-nu integrins with a cyclic RGD peptide impairs angiogenesis, growth and metastasis of solid tumours in vivo. Br J Cancer. 2002; 86(5): 788-95.

47. Janssen ML, Oyen WJ, Dijkgraaf I, Massuger LF, Frielink C, Edwards DS, Rajopadhye M, Boonstra H, Corstens FH, Boerman OC. Tumor targeting with radiolabeled alpha(v)beta(3) integrin binding peptides in a nude mouse model. Cancer Res. 2002; 62(21): 6146-51.

48. Seya T, Matsumoto M, Tsuji S, Begum NA, Azuma I, Toyoshima K. Structural-functional relationship of pathogen-associated molecular patterns: lessons from BCG cell wall skeleton and mycoplasma lipoprotein M161Ag. Microbes Infect. 2002; 4(9): 955-61.







## Figure Legends

Fig. 1 The structure of the adjuvant developed in the present study, a synthetic Toll-like receptor 2 ligand containing the RGDS motif.

(a) The structure of MALP-2. The N-terminal cysteine of a peptide derived from a mycobacterium is modified with 2 palmitates (Pam2Cys, P2C). RGDS was conjugated to P2C to form P2C-RGDS because of its hydrophilicity and its additional function as an integrin-binding motif for cell adhesion. (b) The structure, molecular weight, isoelectric point (pI), and hydrophobicity of synthetic (P2C-RGDS, P2C-SKKKK) and natural (MALP-2, FSL-1) lipopeptides used in this study. The pI and hydrophobicity of the peptide were calculated using ProtParam tools (http://br.expasy.org/tools/protparam.html). The pI and hydrophobicity of P2C-RGDS were almost equivalent to those of MALP-2. The molecular weight of P2C-RGDS was about half that of MALP-2. N: natural TLR2 ligand, S: synthetic TLR2 ligand. The asterisks (*) indicate acidic peptides. The gray boxes indicate hydrophobic amino acids.

Fig. 2 P2C-RGDS activates bone marrow–derived dendritic cells (BMDCs) as much as MALP-2 *in vitro*.

(a) The enhancement of CD80/CD86 expression of BMDCs stimulated with the indicated compounds (100 nM) for 24 h was observed by FACS analysis.

P2CR, P2C-RGDS. (b) IL12p40 and TNF-α production in BMDCs stimulated with each compound for 48 h was determined by ELISA. (c) The proliferation of allogeneic T cells co-cultured with activated-BMDCs for 72 h was measured with the [$^3$H] thymidine uptake method. BMDCs were treated with each compound for 24 h before co-culture with T cells. CPM, count per minute. $^{**}P < 0.01$ vs. control (student t-test)

Fig. 3 P2C-RGDS activates BMDCs in a TLR2 and MyD88-dependent manner *in vitro*.

(a) and (b) BMDCs were prepared from mice lacking TLR2 (TLR2$^{-/-}$) and TLR adaptor molecules (MyD88$^{-/-}$ and TICAM-1$^{-/-}$). CD80 and CD86 expression were observed by FACS analysis at 24 h after BMDCs were stimulated with MALP-2 or P2C-RGDS. The numbers in the panels represent mean fluorescence intensities. P2C-RGDS and MALP-2 activated BMDCs via TLR2 and MyD88, but not via the TICAM-1 pathway.

Fig. 4 P2C-RGDS efficiently activates BMDCs in an RGDS motif–dependent manner *in vitro* over short incubation times.

(a) IL12p40 production of BMDCs stimulated with each TLR2 ligand at 4°C for 1 h. BMDCs were washed after the stimulation and re-cultured for 48 h. IL12p40 production was determined by ELISA. (b) BMDCs were pretreated







with the indicated concentrations of RGDS peptide (P2C-modification free) as a competitor at 4°C for 30 min. Then, the BMDCs were stimulated with TLR2 ligands (10 nM) at 4°C for 1 h. IL12p40 production by BMDCs was determined by ELISA. Data are shown as percentages of each control value. (c) The inhibition effects of α-CD29 (integrin β1) antibody on IL12p40 production of BMDCs. BMDCs were pre-treated with 10μg/ml of each antibody at 4°C for 30 min before stimulation.

Fig. 5 P2C-RGDS efficiently activates splenocytes in an RGDS motif–dependent manner.

(a) IFN-γ production by splenocytes stimulated with each compound for 72 h.

(b) The effect of RGDS competitor peptide pretreatment on IFN-γ production. The RGDS competitor attenuated IFN-γ production from splenocytes stimulated with P2C-RGDS at 4°C for 1 h. (c) The roles of CD11c-positive cells (DCs) and CD90-positive cells (T cells) on IFN-γ production by splenocytes. The splenocytes were separated into CD11c$^+$ and CD11c$^-$ cells, or CD90$^+$ and CD90$^-$ cells by using MACS beads. Cells were prepared based on the recovery ratio and stimulated with P2C-RGDS for 72 h. $^{*}P < 0.05$, $^{**}P < 0.01$ (student t-test); n.d, not detected. (d) Intracellular IFN-γ staining of splenocytes with various expression markers. Density plots show the

expression of each surface marker and intracellular staining for IFN-γ, and the numbers indicate the proportion of IFN-γ positive cells (%).

Fig. 6 P2C-RGDS is more effective at retarding tumor growth and inducing CD8-positive cells than MALP-2 *in vivo* and *ex vivo*.

Antitumor effect of P2C-RGDS and MALP-2 (a), and of a mixture of P2C and RGDS peptide (b), in the EG7-implanted mouse model (C57BL6-EG7 model). Mice were treated with TLR2 ligand and EG7 lysate on days 16, 20, and 23 (arrows). The data are shown as means ± s.e. (n=9). $*P < 0.05$ vs. control (student t-test). (c) Lymph node cells derived from P2C-RGDS and EG7 lysate–immunized mice showed stronger cytotoxicity than cells from MALP-2–immunized mice against EG7 but not B16 ($^{51}$Cr release assay). $*P < 0.05$ vs. MALP2 (student t-test). (d) CD8-positive T cells were more effectively induced in lymph nodes derived from mice immunized with P2C-RGDS and EG7 lysate than in those immunized with MALP-2. The lymph node cells in Fig. 6c were cultured with live EG7 for 96 h, and then the proportion of CD8-positive T cells was analyzed. (e) Immunization with P2C-RGDS and EG7 lysate induced CD8-positive T cells in splenocytes more efficiently than immunization with MALP-2. The proportions of CD8-positive cells in splenocytes were determined by FACS analysis at 96 h after the initiation of splenocyte cultivation. Each symbol indicates an individual







experiment. The closed squares represent average ± s.d. $*p<0.05$ (paired t-test).

(f) The proportion of CD11c-positive cells in the draining lymph nodes at 24 h after immunization. CD11c-positive cells were examined by FACS analysis. $*P = 0.055$ vs. MALP2 (student t-test).

Fig.1

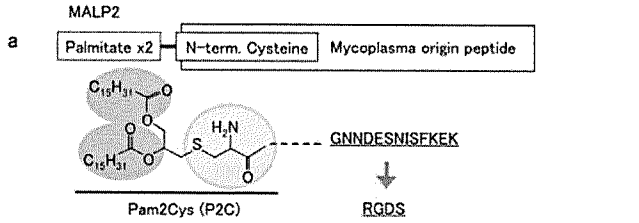


b

| Compounds | | M.W. | Peptide | pI | hydrophobicity |
|---|---|---|---|---|---|
| P2C | | 672.5 | P2 C | — | — |
| MALP2 | (N) | 2134.1 | P2 C G N N D E S N I S F K E K | *4.68 | −1.5 |
| FSL-1 | (N) | 1666.1 | P2 C G D P K H P K S F | 8.21 | −1.36 |
| P2C-SKKKK | (S) | 1271.8 | P2 C S K K K K | 10.04 | −2.32 |
| P2C-RGDS | (S) | 1087.5 | P2 C R G D S | *5.83 | −1.34 |

The structure of the adjuvant developed in the present study, a synthetic Toll-like receptor 2 ligand containing the RGDS motif.
180x107mm (300 x 300 DPI)









Fig.2

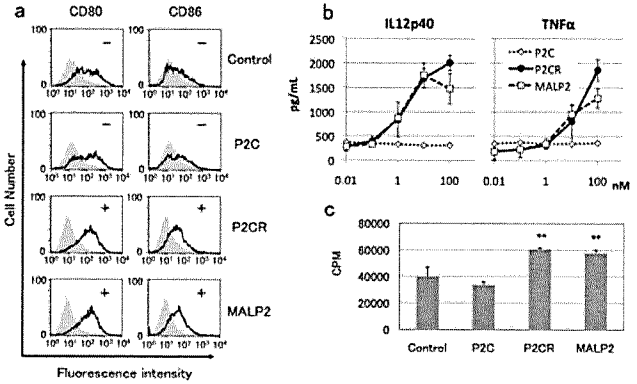


P2C-RGDS activates bone marrow-derived dendritic cells (BMDCs) as much as MALP-2 in vitro.
180x112mm (300 x 300 DPI)

Fig.3

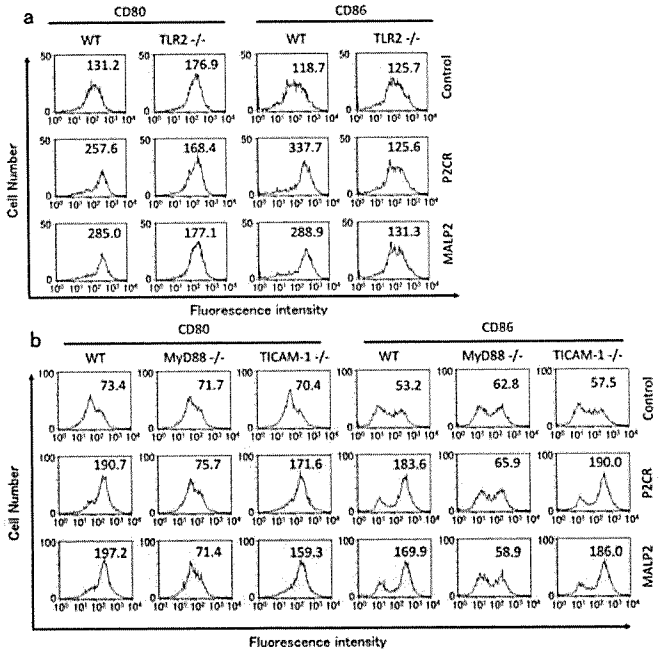


P2C-RGDS activates BMDCs in a TLR2 and MyD88-dependent manner in vitro.
180x191mm (300 x 300 DPI)







Fig.4

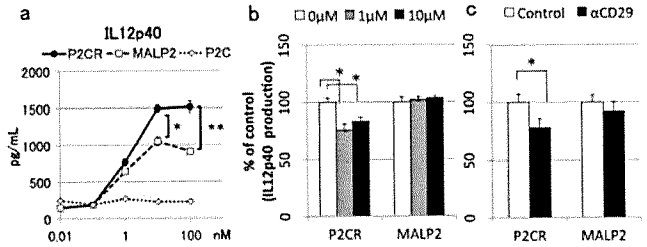


P2C-RGDS efficiently activates BMDCs in an RGDS motif-dependent manner in vitro over short incubation times.
180x79mm (300 x 300 DPI)

Fig.5

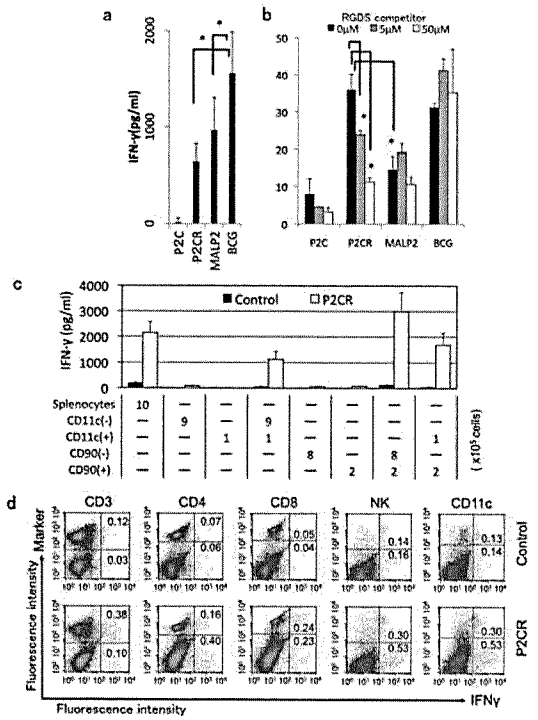


P2C-RGDS efficiently activates splenocytes in an RGDS motif-dependent manner in vitro over short incubation times.
180x254mm (300 x 300 DPI)







Fig.6

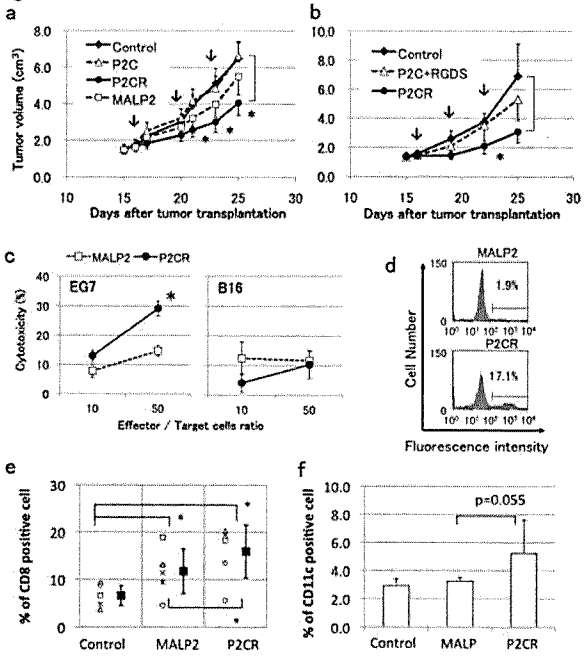


P2C-RGDS is more effective at retarding tumor growth and inducing CD8-positive cells than MALP-2 in vivo and ex vivo
180x189mm (300 x 300 DPI)

THE JOURNAL OF BIOLOGICAL CHEMISTRY VOL. 285, NO. ??, pp. 1–xxx, ???? ??, 2010


# A Molecular Mechanism for Toll-IL-1 Receptor Domain-containing Adaptor Molecule-1-mediated IRF-3 Activation*[S]

Received for publication, December 24, 2009, and in revised form, March 25, 2010 Published, JBC Papers in Press, April 23, 2010, DOI 10.1074/jbc.M109.099101

**Megumi Tatematsu[‡], Akihiro Ishii[‡1], Hiroyuki Oshiumi[‡], Masataka Horiuchi[§], Fuyuhiko Inagaki[§], Tsukasa Seya[‡], and Misako Matsumoto[‡2]**

*From the [‡]Department of Microbiology and Immunology, Hokkaido University Graduate School of Medicine, Kita 15, Nishi 7, Kita-ku Sapporo 060-8638 and the [§]Department of Structural Biology, Graduate School of Pharmaceutical Science, Hokkaido University, N-21, W-11, Kita-ku, Sapporo 001-0021, Japan*

**The Toll-IL-1 receptor (TIR) domain-containing adaptor molecule-1 (TICAM-1, also called TRIF) is a signaling adaptor for TLR3 and TLR4 that activates the transcription factors IRF-3, NF-κB, and AP-1, leading to induction of type I interferon and cytokines. The N-terminal region of TICAM-1 participates in IRF-3 activation, although the C-terminal region is involved in NF-κB activation. However, the mechanism by which TICAM-1 is activated and transmits signals is largely unknown. In this study, we identified Leu[194] as a critical amino acid for TICAM-1-mediated IRF-3 activation. When Leu[194] was substituted with Ala, the mutant TICAM-1 failed to recruit the IRF-3 kinase TBK1, resulting in lack of IRF-3 phosphorylation, although TRAF3 and NAP1 appeared to be recruited. The N-terminal 176 amino acids of TICAM-1 (N-terminal domain (NTD)) form a protease-resistant structural domain. A TICAM-1 mutant lacking the N-terminal 180 amino acids showed greater interferon-β promoter activation than wild-type TICAM-1. Furthermore, immunoprecipitation and protein-protein interaction analysis revealed that the NTD interacted with the N terminus of TICAM-1-TIR. These results suggest that the NTD folds into the TIR domain structure to maintain the naive conformation of TICAM-1. Upon stimulation of TLR3/4, TICAM-1 oligomerizes through the TIR domain and the C-terminal region, which may break the intramolecular association and induce a conformational change that allows TBK1 access to TICAM-1.**

The innate immune system senses microbial infection using Toll-like receptors and cytoplasmic pattern-recognition receptors, which rapidly induce an antimicrobial response (1). Recent studies have demonstrated that these receptors also recognize molecular patterns associated with tissue damage and induce cytokine and chemokine production, which may lead to a sterile inflammation and progression of autoimmune diseases (2). Downstream of each pattern-recognition receptor is a signaling adaptor protein that determines the nature of response by activating distinct transcription factors (3). The Toll-IL-1 receptor (TIR)[3] domain-containing adaptor molecule-1 (TICAM-1), which is also known as TIR domain-containing adaptor inducing IFN-β (TRIF), is a signaling adaptor for TLR3 and TLR4 that activates the transcription factors IRF-3, NF-κB, and AP-1, leading to induction of type I IFN and cytokines, as well as myeloid dendritic cell (mDC) maturation (4–7). The final response mediated by TICAM-1 depends on the cell type and the activating TLR3/4 ligand.

Poly(I-C) is a synthetic analog of viral double strand RNA that generates a unique maturation stage in mDCs via TLR3-TICAM-1-dependent gene expression, leading to activation of natural killer cells and cytotoxic T lymphocytes (8, 9). Monophosphoryl lipid A is a TLR4 ligand that activates mDCs to induce T cell immunity via TICAM-1 but not MyD88 (10), implying that TICAM-1 signaling is crucial for inducing effective cellular responses. In contrast, oxidized phospholipids generated by oxidative stress or virus infection activate cytokine production in lung macrophages through the TLR4-TICAM-1 pathway, and this is the key disease pathway in acute lung injury (11). Thus, specific stimuli have been discovered, but the mechanism by which TICAM-1 is activated by upstream pattern-recognition receptors and transmits downstream signals is largely unknown.

TICAM-1 is expressed at a low level in most tissues and cells and is diffusely localized in the cytoplasm of resting cells (4, 12). When endosomal TLR3 is activated by double strand RNA, TICAM-1 transiently colocalizes with TLR3 and then dissociates from the receptor and forms speckled structures that colocalize with downstream signaling molecules (12, 13). Upon

* This work was supported in part by grants-in-aid from the Ministry of Education, Science, and Culture, the Ministry of Health, Labor, and Welfare of Japan, The NorthTec Foundation, The Akiyama Life Science Foundation, Sapporo Biocluster "Bio-S" (Knowledge Cluster Initiative of Ministry of Education, Culture, Sports, Science and Technology), and the Program of Founding Research Centers for Emerging and Reemerging Infectious Diseases, Ministry of Education, Culture, Sports, Science and Technology.

[S] The on-line version of this article (available at http://www.jbc.org) contains supplemental Figs. 1 and 2.

[1] Present address: Dept. of Global Epidemiology, Hokkaido University Research Center for Zoonosis Control, Kita-20, Nishi-10, Kita-ku, Sapporo, 001-0020, Japan.

[2] To whom correspondence should be addressed. Tel.: 81-11-706-6056; Fax: 81-11-706-7866; E-mail: matumoto@pop.med.hokudai.ac.jp.

[3] The abbreviations used are: TIR, Toll-IL-1 receptor; DAPI, 4′,6-diamidine-2′-phenylindole dihydrochloride; mDC, myeloid dendritic cell; NTD, N-terminal domain (1–176 aa); RHIM, RIP homotypic interacting motif; TRAF, tumor necrosis factor receptor-associated factor; TRIF, TIR domain-containing adaptor-inducing IFN-β; aa, amino acid; PBS, phosphate-buffered saline; HA, hemagglutinin; IFN, interferon; Ab, antibody; mAb, monoclonal antibody; pAb, polyclonal antibody.

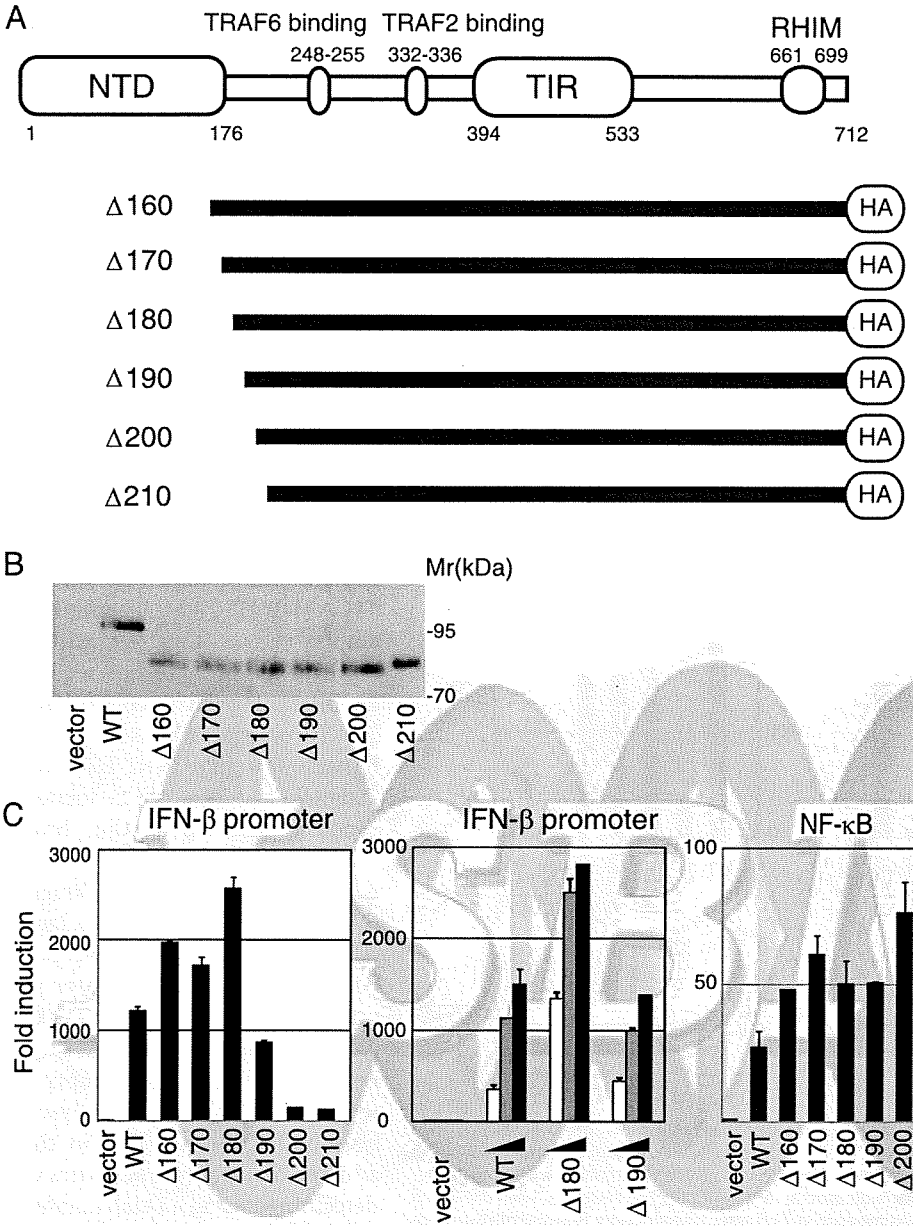


FIGURE 1. **TICAM-1 N-terminal region (191–200 aa) is essential for activation of the IFN-β promoter but not NF-κB.** *A*, schematic structure of human TICAM-1/TRIF and TICAM-1 mutants. *B*, protein expression of truncated TICAM-1 mutants in HEK293 cells. HEK293 cells in 24-well plates were transfected with the expression plasmids for HA-tagged wild-type TICAM-1 or TICAM-1 mutants (100 ng). Protein expression levels were determined by immunoblotting using anti-HA pAb. *C*, functional analysis of TICAM-1 mutants. HEK293 cells were transfected with empty vector or expression plasmid for wild-type (*WT*) TICAM-1 or each TICAM-1 mutant (Δ160–Δ210) (100 ng) together with the IFN-β promoter reporter (*left panel*) or NF-κB reporter plasmid (*right panel*), and phRL-TK. In some experiments, HEK293 cells were transfected with increasing amounts of expression vectors (10, 50, and 100 ng) (*center panel*). Luciferase activity was measured 24 h after transfection. Representative data from a minimum of four separate experiments, each performed in triplicate, are shown.

lipopolysaccharide stimulation, TICAM-1 is activated by endosomal TICAM-2 (also called TRIF-related adaptor molecule), which associates with the internalized TLR4 (14). Forced expression of TICAM-1 leads to homo-oligomerization through the TIR domain and the C terminus, forming a complex called the TICAM-1 signalosome (15). The TIR domain of TICAM-1 is essential for binding to the TIR domain of TLR3 and to TICAM-2. The N-terminal region of TICAM-1 participates in IRF-3 activation by recruiting the IRF-3-activating kinases, TANK-binding kinase 1 (TBK1) and inhibitor of nuclear factor κB kinase ϵ (also called IKKι) (16–18). The C-terminal region of TICAM-1 is involved in NF-κB activation and inducing apoptosis by binding the RIP1 at the receptor-interacting protein homotypic interacting motif (RHIM) domain (19, 20). The tumor necrosis factor receptor-associated factor (TRAF) 3 and NF-κB-activating kinase-associated protein 1 (NAP1) engage in TICAM-1-mediated activation of IRF-3 (21–23). Thus, although molecules involved in the TICAM-1-mediated signaling have been identified, the molecular mechanism for TICAM-1 activation remains unknown.

Recently, the N-terminal 176 amino acids (aa) of TICAM-1 (NTD) were found to form a protease-resistant structure of eight α-helices (24). In this study, we analyzed the structure-function relationship of TICAM-1 with a series of TICAM-1 mutants and identified the critical amino acid for TICAM-1-mediated IRF-3 activation. Moreover, we offer a structural model of the resting form of TICAM-1, in which NTD folds into the TIR domain structure, preventing homodimerization and access of downstream signaling molecules to TICAM-1.

## EXPERIMENTAL PROCEDURES

*Cell Culture and Reagents*—HEK293 cells were maintained in Dulbecco's modified Eagle's medium low glucose (Invitrogen) supplemented with 10% heat-inactivated fetal calf serum (BIOSOURCE) and antibiotics. HEK293FT cells were maintained in Dulbecco's modified Eagle's medium high glucose supplemented with 0.1 mM nonessential amino acids, 10% heat-inactivated fetal calf serum, and antibiotics. HeLa cells were maintained in minimum essential media (Nissui, Tokyo, Japan) supplemented with 1% L-glutamine and 5% heat-inactivated fetal calf serum. Anti-FLAG M2 mAb, anti-HA pAb, 4′,6-diamidine-2′-phenylindole dihydrochloride (DAPI), and benzyloxycarbonyl-VAD-fluoromethyl ketone were from Sigma. Alexa Fluor®-conjugated secondary antibodies were from Invitrogen; anti-Myc mAb was from Neomarkers (Lab Vision

balt3/zbc-bc/zbc-bc/zbc02810/zbc2168-10z ZSUBMIT 15 xppws S=1 13/5/10 4:21 | 4/Color Figure(s) F4,6,7 | ARTNO: M109.099101



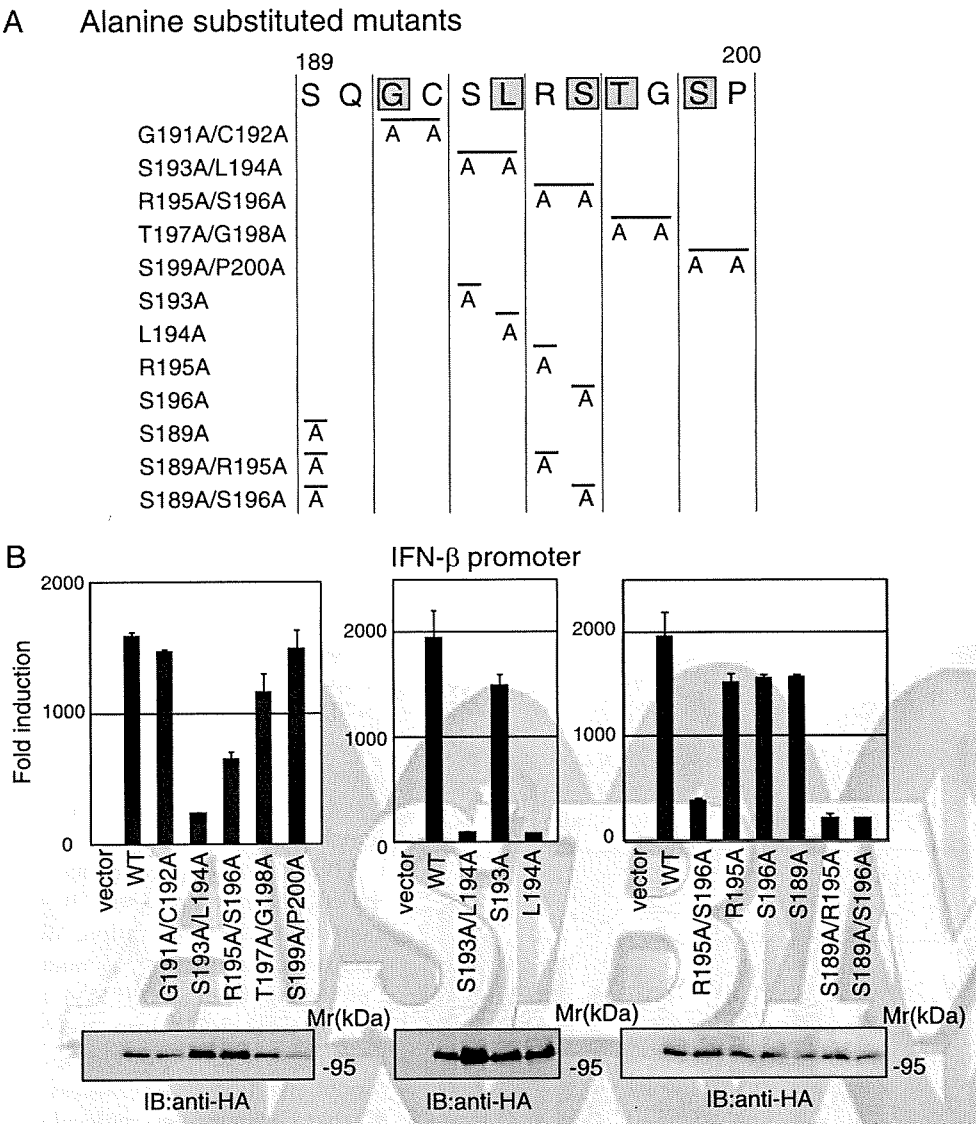


FIGURE 2. **Leu[194] is critical for TICAM-1-mediated IFN-β promoter activation.** *A*, amino acid sequence between Ser[189] and Pro[200] in TICAM-1. *Gray* indicates conserved residues between human and mouse. *B*, IFN-β promoter activation by alanine-substituted TICAM-1 mutants. HEK293 cells were transfected with empty vector or expression vectors for wild-type (*WT*) TICAM-1 or indicated alanine-substituted mutants, with the IFN-β promoter reporter and phRL-TK. Luciferase activity was measured 24 h after transfection. Representative data from a minimum of three separate experiments, each performed in triplicate, are shown. *Lower panels*, protein expression of alanine-substituted mutants in HEK293 cells. Cell lysates prepared in *A* were subjected to SDS-PAGE (7.5% gel) followed by immunoblotting (*IB*) with anti-HA pAb.

Corp., Fremont, CA); anti-HA mAb was from Covance (Emeryville, CA); anti-TBK1 pAb was from Abcam (Cambridge, MA); anti-human IRF3 rabbit IgG was from IBL (Gunma, Japan); horseradish peroxidase-conjugated secondary Abs were from BIOSOURCE; and poly(I-C) was from GE Healthcare.

*Plasmids*—Complementary DNAs for human TICAM-1, RIP1, TRAF2, TRAF3, and TRAF6 were cloned in our laboratory by reverse transcription-PCR and ligated into the cloning site of the expression vectors, pEF-BOS and p3×FLAG-CMV-14 (C-terminal 3×FLAG tag) (15). The pCDNA3.1/NAP1-Myc and pCDNA3.1/TBK1-FLAG expression vectors were kindly provided by Dr. M. Nakanishi (Nagoya City University, Nagoya, Japan). N-terminal deletion mutants of TICAM-1 (Δ160, Δ170, Δ180, Δ190, Δ200, and Δ210) were made by PCR with *Pfu* Turbo DNA polymerase (Stratagene, La Jolla, CA) using appropriate primers. pEF-BOS/TICAM-1-HA was used as a PCR template (33). Point mutations in TICAM-1 were generated by site-directed mutagenesis. Truncated TICAM-1 mutants TICAM-1-NTD (1–176 aa), TICAM-1-N (1–359 aa), TICAM-1-TIR (387–556 aa), and TICAM-1-C (534–712 aa) were generated by PCR using specific primers. An HA tag was inserted at the C terminus of each mutant.

*Reporter Gene Assays*—HEK293 cells ($2 \times 10^5$ cells/well) cultured in 24-well plates were transfected with expression vectors for wild-type TICAM-1, TICAM-1 mutants, or empty vector, together with the reporter plasmid (100 ng/well) and an internal control vector, phRL-TK (Promega, Madison, WI) (5 ng/well) using FuGENE HD (Roche Diagnostics). The p-125 luciferase reporter contained the human IFN-β promoter (−125 to +19) and was provided by Dr. T. Taniguchi (University of Tokyo, Tokyo, Japan). A luciferase-linked NF-κB reporter gene and pAP-1-Luc reporter plasmid were from Stratagene. The total amount of DNA (500 ng/well) was kept constant by adding empty vector. After 24 h, cells were lysed in lysis buffer (Promega), and firefly and *Renilla* luciferase activities were determined using a Dual-Luciferase reporter assay kit (Promega). The firefly luciferase activity was normalized to the *Renilla* activity and expressed as the fold-stimulation relative to the activity of vector-transfected cells. All assays were performed in triplicate.

*Confocal Microscopy*—HeLa cells ($1.0 \times 10^5$ cells/well) were plated onto micro cover glasses (Matsunami, Tokyo, Japan) in 12-well plates. The next day, cells were transfected with the indicated plasmids as above. For cells transfected with wild-type TICAM-1 or the L194A mutant, benzyloxycarbonyl-VAD-fluoromethyl ketone (20 μM) was added to the cells before transfection to inhibit apoptosis. 24 h after transfection, cells were fixed in acetone for 3 min and permeabilized with PBS containing 0.2% Triton X-100 for 10 min. Fixed cells were blocked in phosphate-buffered saline (PBS) containing 1% bovine serum albumin and labeled with the indicated primary Abs (3.0 μg/ml) for 60 min at room temperature. For staining endogenous TBK1, cells were fixed with 4% paraformaldehyde

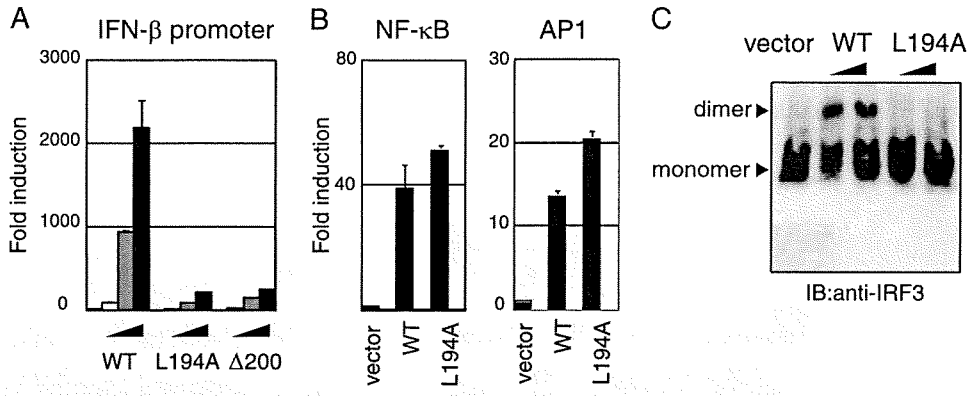


FIGURE 3. **Leu[194] is critical for TICAM-1-mediated IRF-3 activation.** *A*, L194A mutant lost IFN-β promoter-activating ability. HEK293 cells were transfected with increasing amounts of wild-type (*WT*) TICAM-1 or L194A mutant expression vector (1, 10, and 100 ng) with an IFN-β reporter and phRL-TK. Luciferase activity was measured 24 h after transfection. Representative data from a minimum of three separate experiments are shown. *B*, L194A mutant activates NF-κB and AP-1. HEK293 cells were transfected with wild-type TICAM-1 or L194A mutant expression vector (100 ng) together with NF-κB (*left panel*) or AP-1 (*right panel*) reporters. *C*, L194A lost IRF-3 activating ability. HEK293 cells were transfected with empty vector, wild-type TICAM-1 vector, or L194A vector (100 and 400 ng). After 24 h, lysates were prepared and subjected to native PAGE. Monomeric and dimeric forms of IRF-3 (*arrowheads*) were detected by Western blot. *IB*, immunoblot.

for 10 min. Endogenous TBK1 was labeled with anti-TBK1 pAb (1:500). Alexa Fluor 488- or 594-conjugated secondary Abs (1:400) were used to visualize the primary Abs. Nuclei were stained with DAPI (2 μg/ml) in PBS for 10 min before mounting onto glass slides using PBS with 2.3% 1,4-diazabicyclo[2.2.2]octane and 50% glycerol. Cells were visualized at a 63× magnification with an LSM510 META microscope (Zeiss, Jena, Germany).

*Immunoprecipitation and Immunoblotting*—HEK293FT cells ($5 \times 10^5$ cells/well) cultured in 6-well plates were transfected as above with the indicated plasmids. For wild-type TICAM-1 and the TICAM-1 mutants containing the RHIM domain, benzyloxycarbonyl-VAD-fluoromethyl ketone (20 μM) was added as described above. The total amount of DNA (2.0 μg/well) was kept constant with an empty vector. After 24 h, cells were lysed in lysis buffer (20 mM Tris-HCl, pH 7.5, containing 150 mM NaCl, 1% Nonidet P-40, 10 mM EDTA, 25 mM iodoacetamide, 2 mM phenylmethylsulfonyl fluoride, 5 mM $Na_3VO_4$ and a protease inhibitor mixture (Roche Diagnostics)). Lysates were pre-cleared with ;Protein G-Sepharose (GE Healthcare) and incubated with 0.5 μg of anti-tag Abs or anti-TBK1 pAb (1:50). Immunocomplexes were recovered by incubation with protein G-Sepharose, washed five times with lysis buffer, and resuspended in denaturing buffer. Samples were analyzed by SDS-PAGE (7.5–12.5% gel) under reducing conditions followed by immunoblotting with anti-tag Abs. For immunoblotting, HEK293 cells cultured in 24-well plates were transfected with the indicated plasmids (100 ng). After 24 h, cells were lysed in lysis buffer. Lysates were clarified by centrifugation and subjected to SDS-PAGE (7.5% gel) followed by immunoblotting with anti-HA pAb.

*Assay for IRF-3 Activation*—HEK293 cells ($2 \times 10^5$ cells/well) cultured in 24-well plates were transfected with wild-type TICAM-1 or TICAM-1 L194A mutant (0.1 and 0.4 μg) using Lipofectamine 2000 reagent (Invitrogen). The total amount of DNA (0.8 μg/well) was kept constant with an empty vector. After 24 h, cells were lysed in lysis buffer (50 mM Tris-HCl, pH 8.0, containing 150 mM NaCl, 1% Nonidet P-40, 100 ng/ml leupeptin, 1 mM phenylmethylsulfonyl fluoride, and 5 mM $Na_3VO_4$). Lysates were clarified by centrifugation (15,000 rpm, 10 min) and subjected to native-PAGE (7.5% gel) as described previously (34). Immunoblotting was performed using rabbit anti-human IRF-3 antibody and horseradish peroxidase-conjugated goat anti-rabbit IgG.

*Protein-Protein Interaction Analysis*—Protein-protein association in living cells was analyzed using the CoralHue Fluo-chase kit (MBL, Nagoya, Japan), which detects protein-protein interactions as fluorescent signals using the protein fragment complementation method. TICAM-1 NTD and TICAM-1-TIR cDNAs were subcloned into fusion protein expression plasmids according to the manufacturer's instructions. The *TICAM-1* NTD gene was fused to the 3′-end of the divided monomeric Kusabira-Green (*mKG*) gene N- or C-terminal fragment (mKGN-NTD and mKGC-NTD), and the *TICAM-1*-TIR gene was fused to the 5′- or 3′-end of the *mKG* gene N- or C-terminal fragment (TIR-mKGN, TIR-mKGC, mKGN-TIR, and mKGC-TIR). HEK293FT cells ($5 \times 10^5$ cells/well) cultured in 6-well plates were transfected with the indicated combinations of plasmids as above. After 24 h, the conditioned media were replaced with Dulbecco's PBS, and fluorescent living cells were visualized with fluorescent microscopy (Olympus).

## RESULTS

*TICAM-1 N Terminus from Gly[191] to Pro[200] Is Essential for IFN-β Promoter Activation*—The N terminus of TICAM-1 contains TRAF6- and TRAF2-binding sites (Fig. 1*A*). Limited F1
trypsin digestion of TICAM-1 (1–556 aa) for 4 h generates the N-terminal fragment TICAM-1(1–176), and 20 h of digestion yields the fragment TICAM-1(1–156) (24). To examine the role of the TICAM-1 N-terminal domain, we made a series of truncated constructs (Δ160–Δ210) and assayed NF-κB and IRF-3 activation by reporter assay. The protein expression levels of these mutants were approximately equivalent to wild type (Fig. 1*B*). TICAM-1-mediated IFN-β promoter activation was enhanced by deletion of the N-terminal 160, 170, or 180 aa, whereas the TICAM-1-mutant lacking the N-terminal 190 aa (Δ190) showed less activity than wild-type TICAM-1 (Fig. 1*C*, *left* and *center panels*). Interestingly, a TICAM-1 mutant lacking the N-terminal 200 or 210 aa (Δ200, Δ210) showed dramatic loss of activity. NF-κB activation ability, however, was enhanced in all the mutants (Fig. 1*C*, *right panel*). These results indicated that the N-terminal amino acids between Gly[191] and Pro[200] are essential for TICAM-1-mediated IFN-β promoter activation but not for NF-κB activation.

balt3/zbc-bc/zbc-bc/zbc02810/zbc2168-10z ZSUBMIT 15 xppws S=1 13/5/10 4:21 | 4/Color Figure(s) F4,6,7 | ARTNO: M109.099101



*Leu*$^{194}$ *Is Critical for TICAM-1-mediated IFN-β Promoter Activation*—To identify residues crucial for TICAM-1-mediated IFN-β promoter activation, we performed alanine scanning of the region between Gly$^{191}$ and Pro$^{200}$ (Fig. 2*A*). Alanine-substituted mutants were expressed in HEK293 cells with an IFN-β reporter gene, and IFN-β promoter activation was assessed after 24 h. Western blot showed that the mutated proteins were expressed at levels similar to wild-type TICAM-1 in HEK293 cells (Fig. 2*B*, *lower panels*). Similar to the Δ200 mutant, the S193A/L194A mutant showed no activity, and the R195A/S196A mutant had partially diminished activity (Fig. 2*B*, *left panel*). Other mutations had no effect on the ability to activate the IFN-β promoter. Because substitution of Ser$^{193}$ and Ser$^{196}$ caused dysfunctional mutants, we made the additional single aa-substituted mutants S193A, L194A, R195A, S196A, and S189A and the combinations S189A/R195A and S189A/S196A, and we examined the role of these residues in TICAM-1 signaling (Fig. 2*A*). Remarkably, the substitution of Leu$^{194}$ with Ala completely abolished IFN-β promoter-activation ability, whereas other single aa substitutions only slightly decreased activity. Both S189A/R195A and S189A/S196A mutants showed severely reduced activity (Fig. 2*B*, *center* and *right panels*). These results suggested that Leu$^{194}$ is a critical amino acid for TICAM-1-mediated IFN-β promoter activation and that Ser$^{189}$, Arg$^{195}$, and Ser$^{196}$ near Leu$^{194}$ are associated with this promoter activation.

*Leu*$^{194}$ *Is Indispensable for TICAM-1-mediated IRF-3 Activation*—The L194A mutant did not activate the IFN-β promoter, even though its expression was comparable with wild-type TICAM-1 (Fig. 3*A*). The promoter of the human IFN-β gene possesses binding sites for IRF-3, NF-κB, and AP-1 (25), so we examined which activation pathways were affected by mutation of Leu$^{194}$. As shown in Fig. 3*B*, substitution of Leu$^{194}$ with Ala did not affect NF-κB- and AP-1-activation. In contrast, the ability to activate IRF-3 was abolished in the L194A mutant. Phosphorylation and dimer formation of IRF-3 were induced by the forced expression of wild-type TICAM-1 but not the L194A mutant in HEK293 cells (Fig. 3*C*), which suggested that

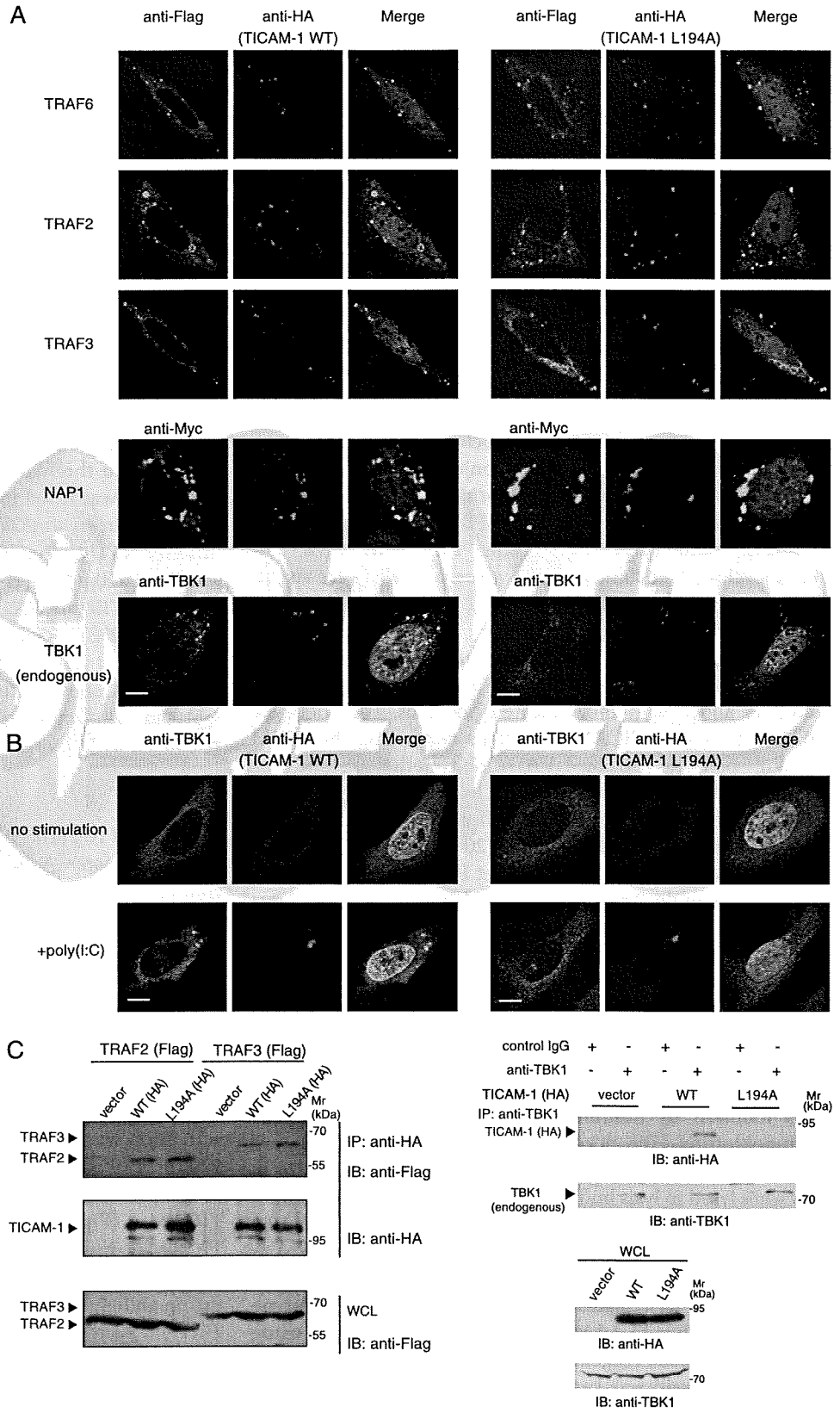

## TBK1 Association Site in TICAM-1/TRIF

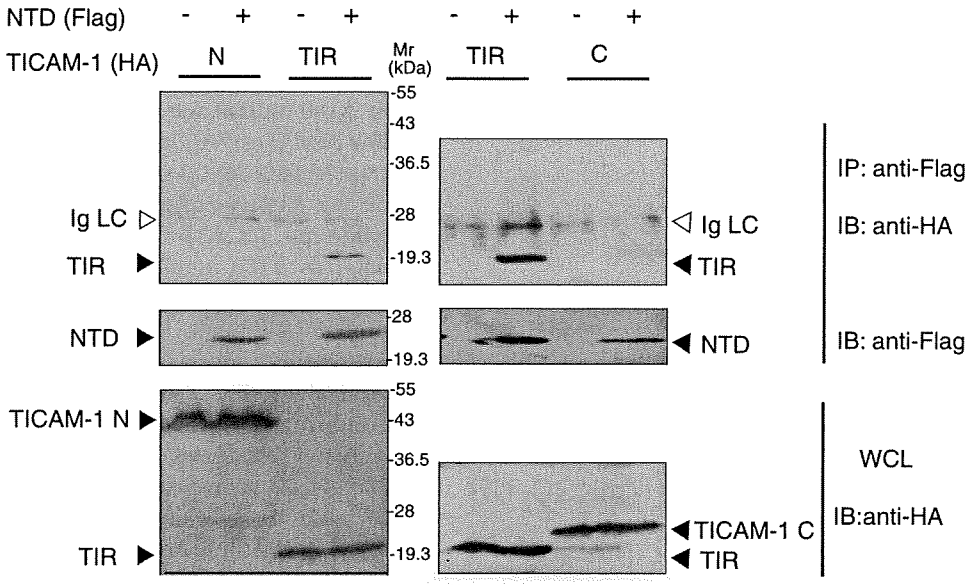


FIGURE 5. **NTD physically associates with TICAM-1-TIR.** HEK293FT cells were transfected with FLAG-tagged NTD and HA-tagged TICAM-1-N (1–359 aa), TIR domain (387–566 aa), or TICAM-1-C (567–712 aa). After 24 h, cells were lysed, and NTD was immunoprecipitated (*IP*) using an anti-FLAG mAb. The immunoprecipitants were resolved on SDS-PAGE (12.5% gel) under reducing conditions followed by immunoblotting (*IB*) with anti-HA pAb or anti-FLAG mAb. Whole cell lysates (*WCL*) were subjected to immunoblotting with anti-HA pAb to detect protein expression. *Open arrowheads* indicate immunoglobulin light chain (*Ig LC*). Molecular weight markers are on the *right*.

$Leu^{194}$ is indispensable for TICAM-1-mediated IRF-3 activation.

*$Leu^{194}$ Is a Critical Amino Acid for Recruitment of TBK1 to TICAM-1*—TRAF3 is an essential signaling molecule for TICAM-1-mediated IRF-3 activation (22, 23), and TRAF6 and TRAF2 directly bind to the N terminus of TICAM-1 through distinct binding sites (26). We analyzed the recruitment of TRAF family members to wild-type TICAM-1 or the L194A mutant by immunofluorescence staining and confocal microscopy. When HeLa cells were cotransfected with expression plasmids for HA-tagged wild-type or mutated TICAM-1, and FLAG-tagged TRAF6, TRAF2, or TRAF3, TRAF proteins colocalized with the L194A mutant as with the wild type (Fig. 4*A*). These results were confirmed by immunoprecipitation (Fig. 4*C*, *left panel*). We next examined whether $Leu^{194}$ is required for recruitment of NAP1 and TBK1. NAP1, which is essential for TICAM-1-mediated IRF-3 activation and functions downstream of TRAF3, colocalized with both wild-type and the L194A mutant (Fig. 4*A*). However, the IRF-3 kinase TBK1 did not colocalize with the L194A mutant.

The lack of association between the L194A mutant and endogenous TBK1 was also observed in TLR3-mediated activation. Wild-type and the L194A mutant diffusely localized in cytoplasm when expressed at a low level (Fig. 4*B*). After poly(I-C) stimulation, wild-type TICAM-1 formed a speckle-like signalosome where endogenous TBK1 colocalized (Fig. 4*B*, *left panels*). In contrast, the L194A mutant did not recruit TBK1 to its signalosome (Fig. 4*B*, *right panels*). We analyzed physical association of TBK1 with wild-type or the L194A mutant by immunoprecipitation. Overexpressed HA-tagged wild-type TICAM-1 was coimmunoprecipitated with endogenous TBK1, although the L194A mutant was not (Fig. 4*C*, *right panels*). These results indicate that $Leu^{194}$ is a key amino acid for recruitment of TBK1.

*TICAM-1 NTD Interacts with the TICAM-1-TIR Domain*—We previously showed that recruitment of NAP1 and TBK1 to TICAM-1 requires homo-oligomerization through the TIR domain and the C terminus and RIP1 binding to the RHIM domain (15). Upon TLR3/4 ligand stimulation, homo-oligomerization is triggered by binding to dimerized TLR3 or TICAM-2, and overexpression of TICAM-1 induces homo-oligomerization (15). How TICAM-1 molecules are prevented from auto-activation in the resting state remains unresolved. TICAM-1 contains two structural domains, the NTD and the TIR domain, and $Leu^{194}$ and the TRAF2/6-binding sites are between these domains. We hypothesized that these interacting sites are covered by the NTD to prevent downstream signaling molecules from accessing TICAM-1.

To test this hypothesis, we investigated the physical association of the NTD with truncated TICAM-1 fragments. FLAG-tagged NTD was coexpressed with HA-tagged TICAM-1-N, TICAM-1-TIR, or TICAM-1-C in HEK293FT cells, and coimmunoprecipitation was performed using anti-tag Abs. Notably, NTD coimmunoprecipitated with TICAM-1-TIR but

AQ:D FIGURE 4. **$Leu^{194}$ is indispensable for recruitment of TBK1 to TICAM-1.** *A*, confocal images show HeLa cells coexpressing HA-tagged wild-type (*WT*) TICAM-1 (*left panels*) or L194A mutant (*right panels*) and FLAG-tagged TRAF6, TRAF2, and TRAF3 or Myc-tagged NAP1. HeLa cells, transfected with the expression plasmids for HA-tagged wild-type TICAM-1 or L194A mutant (50 ng) and the indicated FLAG- or Myc-tagged signaling molecules (300 ng), were stained with anti-FLAG or anti-Myc mAb and anti-HA pAb, followed by Alexa Fluor 488-labeled goat anti-mouse Ab and Alexa Fluor 568-labeled goat anti-rabbit Ab. Colocalization of TICAM-1 with endogenous TBK1 was detected using anti-TBK1 pAb and Alexa Fluor 488-labeled goat anti-rabbit Ab. *Red*, wild-type and L194A mutant; *green*, TRAF6, TRAF2, TRAF3, NAP1, and TBK1; *blue*, DAPI-stained nuclei. *Bar*, 10 $\mu$m. *B*, recruitment of endogenous TBK1 to TICAM-1 by poly(I-C) stimulation. HeLa cells were transfected with the expression vector for HA-tagged wild-type TICAM-1 or L194A mutant (0.1 ng). Twenty four hours after transfection, cells were stimulated with buffer alone or 10 $\mu$g/ml poly(I-C) for 30 min. Fixed cells were labeled with anti-HA mAb and anti-TBK1 pAb, followed by Alexa Fluor 568-labeled goat anti-mouse IgG and Alexa Fluor 488-labeled goat anti-rabbit IgG. *C*, endogenous TBK1 physically associates with wild-type TICAM-1 but not the L194A mutant. *Left panels*, HEK293FT cells were transfected with empty vector or expression vectors for HA-tagged wild-type (*WT*) TICAM-1 or L194A mutant together with FLAG-tagged TRAF2, TRAF3. After 24 h, cells were lysed, and TICAM-1 was immunoprecipitated using an anti-HA pAb. *Right panels*, cells were transfected with empty vector or expression vector for HA-tagged wild-type TICAM-1 or L194A mutant. After 24 h, cells were lysed, and endogenous TBK1 was immunoprecipitated (*IP*) using an anti-TBK1 pAb. Rabbit IgG was used as a control Ab. The immunoprecipitants were resolved on SDS-PAGE (7.5% gel) under reducing conditions followed by immunoblotting (*IB*) with anti-tag mAb or anti-TBK1 pAb. Whole cell lysates (*WCL*) were subjected to immunoblotting with anti-FLAG mAb, anti-HA pAb, or anti-TBK1 pAb to detect protein expression (*IB*). Molecular weight markers are on the *right*.

balt3/zbc-bc/zbc-bc/zbc02810/zbc2168-10z ZSUBMIT 15 xppws S=1 13/5/10 4:21 | 4/Color Figure(s) F4,6,7 | ARTNO: M109.099101



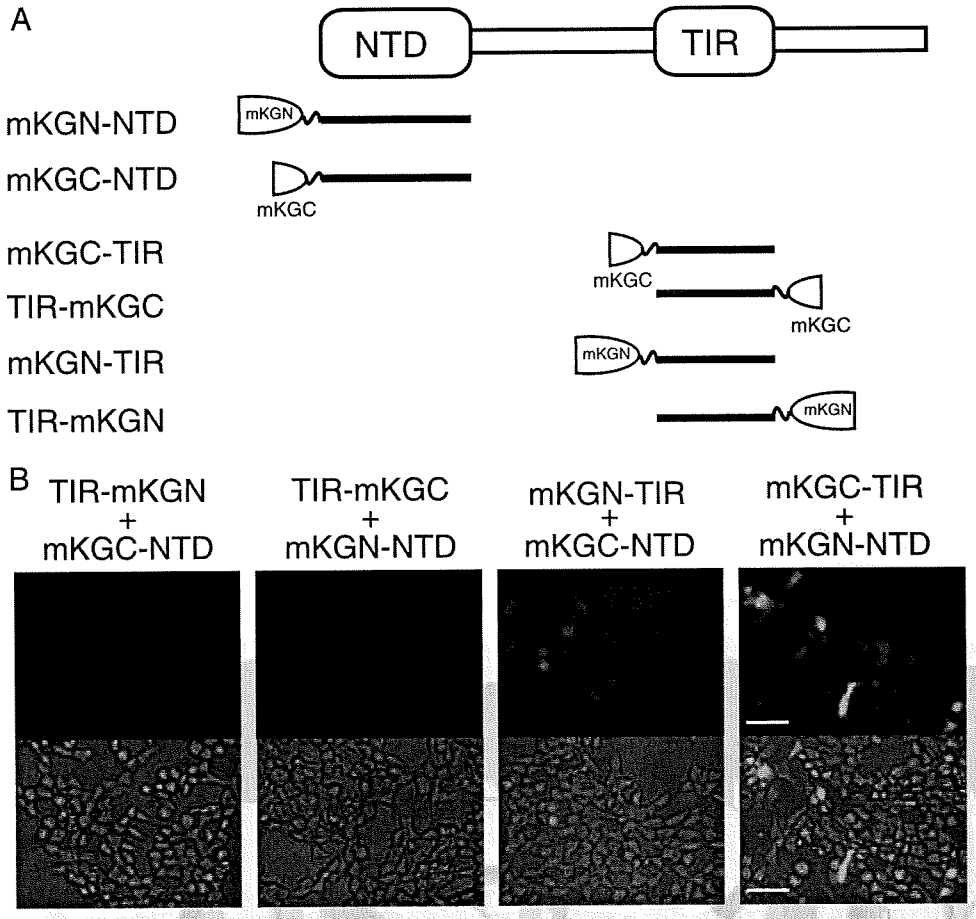


FIGURE 6. **NTD interacts with the N-terminal TICAM-1-TIR.** *A*, NTD or TICAM-1-TIR was fused to mKG fragments. *B*, fluorescence images show HEK293FT cells coexpressing NTD and TICAM-1-TIR, fused to mKG fragments at the N or C terminus. HEK293FT cells were transfected with the indicated combinations of expression plasmids for truncated TICAM-1 mutants fused to mKG fragments (each 500 ng). Twenty four hours after transfection, conditioned media were replaced with Dulbecco's PBS. Cells were visualized by fluorescence microscopy. Signal was detected in cells coexpressing mKGC-TIR and mKGN-NTD, and faint fluorescence was observed in cells coexpressing mKGN-TIR and mKGC-NTD. *Bar*, 100 μm.

not with TICAM-1-N or TICAM-1-C (Fig. 5), suggesting an intramolecular association between the NTD and the TIR domain. To further assess direct interaction between the NTD and the TIR domain, protein-protein interaction analysis was performed using a protein fragment complementation method. We made six constructs fusing the N- or C-terminal fragment of the monomeric Kusabira-Green protein to the N terminus of the NTD (mKGN-NTD, mKGC-NTD), the N terminus of the TIR domain (mKGN-TIR, mKGC-TIR), or the C terminus of the TIR domain (TIR-mKGN, TIR-mKGC) (Fig. 6*A*). Fluorescence was detected when expressed fused proteins interacted, restoring the mKG protein from the mKG fragments. HEK293FT cells were transfected with combinations of expression plasmids, and 24 h after transfection, strong fluorescent signals were detected in cells coexpressing mKGC-TIR and mKGN-NTD, and faint signals were detected in the cells coexpressing mKGN-TIR and mKGC-NTD (Fig. 6*B*). In contrast, cells coexpressing TIR-mKGN or TIR-mKGC and mKG-NTD did not fluoresce (Fig. 6*B*). These results strongly suggested that the NTD interacts with the N-terminal TICAM-1-TIR domain.

A TICAM-1 mutant lacking the NTD (Δ180) had high potential to activate the IFN-β promoter compared with wild-type TICAM-1 (Fig. 1*C*). This augmented activity of Δ180 mutant was more clearly shown when wild-type or Δ180 mutant was expressed at a low level (Fig. 7*A*). In HEK293 cells F7 transfected with 0.1 ng of wild-type- or the L194A-expressing plasmid, wild-type TICAM-1 was inactive, whereas Δ180 mutant exerted the ability to activate the IFN-β promoter, although their protein expression levels were almost equivalent (Fig. 7*B*). Under these conditions, wild-type TICAM-1 diffusely localized in cytoplasm (Fig. 7*C*). In contrast, Δ180 mutant formed a speckle-like signalosome in unstimulated cells as seen in poly(I-C)-stimulated wild-type TICAM-1 (Fig. 7*C*), suggesting that deletion of the NTD facilitates the homo-oligomerization of Δ180 mutant through the TIR domain.

## DISCUSSION

Activation of the transcription factor IRF-3 is a key downstream event in the signaling cascade of TICAM-1, resulting in induction of antiviral genes, including IFN-β. Direct binding of TICAM-1 to the IRF-3 activating kinase TBK1 is necessary for IRF-3 phosphorylation. Here, we identified $Leu^{194}$ as essential in TICAM-1 for recruiting TBK1. Although $Leu^{194}$ was critical for TBK1 binding, $Ser^{189}$, $Arg^{195}$, and $Ser^{196}$ may stabilize the interaction.

TICAM-1 has two structural domains, the NTD and the TIR domain. Results from trypsin digestion of the TICAM-1 (1–566 aa) suggest the region between the NTD and the TIR domain forms a loose structure that might recruit downstream signaling molecules (24). Because the crucial amino acids for TRAF2, TRAF6, and TBK1 binding reside in this region, naive TICAM-1 may have a closed conformation that covers these sites. Indeed, using the protein-protein association analysis, we clearly showed that the NTD interacted with the N-terminal TIR domain. These observations suggest that the NTD folds into the TIR domain, preventing downstream signaling molecules from accessing their binding sites. Upon stimulation of TLR3/4, or TICAM-1 overexpression, TICAM-1 oligomerizes through the TIR domain and the C-terminal region (15). This may break the intramolecular association and induce a conformational change that allows downstream signaling molecules to their binding sites.

Deletion of the NTD augmented the TICAM-1 activity (Fig. 7). The association sites of TRAF2/6 and TBK1 are likely to be available in the Δ180 mutant. This would facilitate recruitment

## TBK1 Association Site in TICAM-1/TRIF

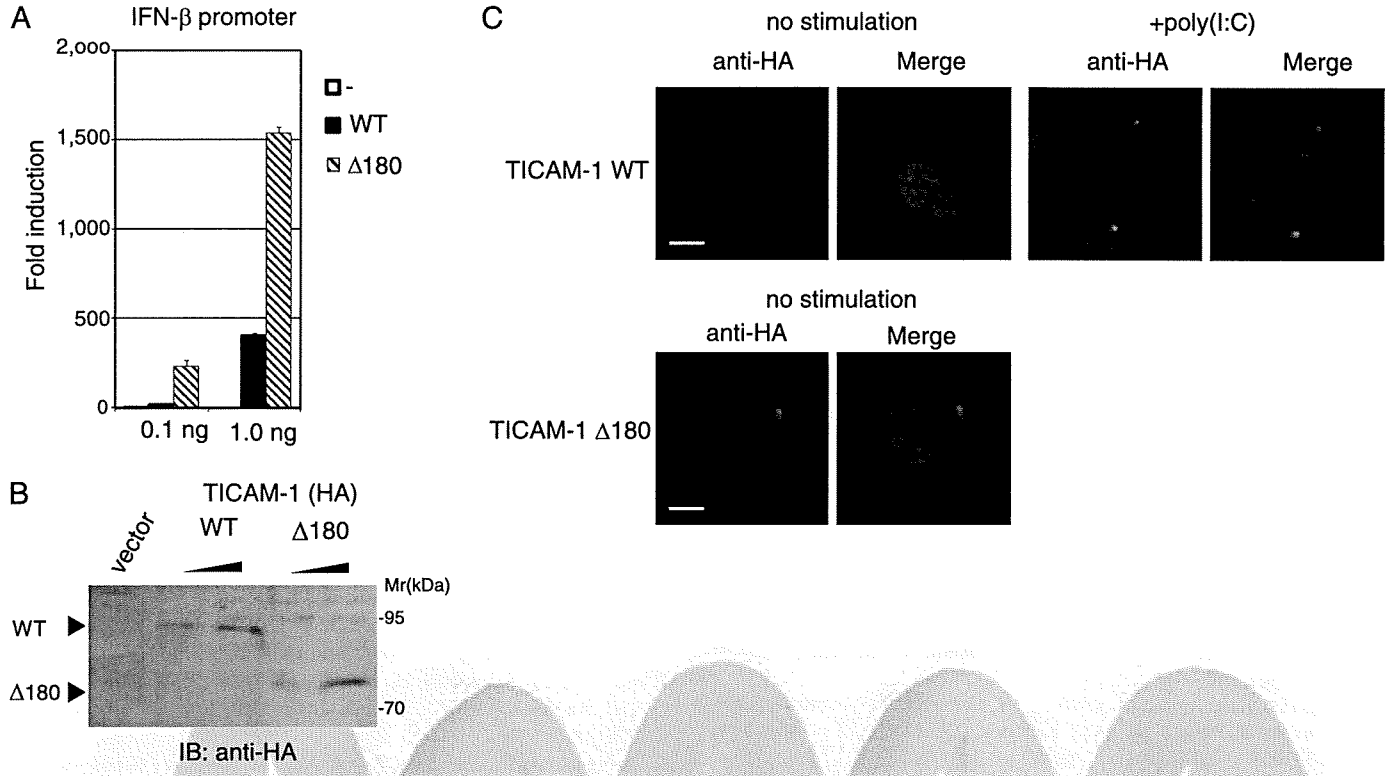


FIGURE 7. **Δ180 mutant had high potential to activate the IFN-β promoter compared with wild-type TICAM-1.** *A*, IFN-β promoter activation by the Δ180 mutant. HEK293 cells were transfected with empty vector or expression plasmid for wild-type (*WT*) TICAM-1 or Δ180 mutant (0.1 and 1.0 ng) together with the IFN-β promoter reporter. Luciferase activity was measured 24 h after transfection. Representative data from a minimum of four separate experiments, each performed in triplicate, are shown. *B*, protein expression of wild-type and the Δ180 mutant in HEK293 cell lysates. *IB*, immunoblot. *C*, confocal images of HeLa cells expressing a low level of HA-tagged wild-type TICAM-1 (*upper panels*) or Δ180 mutant (*lower panels*). Cells were transfected with the expression plasmid for wild-type TICAM-1 or Δ180 mutant (0.1 ng). After 24 h, cells were stimulated with buffer alone or 10 μg/ml poly(I-C) for 30 min, and fixed cells were labeled with anti-HA pAb and Alexa Fluor 568-labeled secondary Ab. The Δ180 mutant formed a speckle-like signalosome in unstimulated cells. *Red*, wild-type and Δ180 mutant; *blue*, DAPI-stained nuclei. *Bar*, 10 μm.

of the IRF-3 kinase complex. The Δ190 mutant showed reduced IFN-β promoter activation compared with the Δ180 mutant, probably because the absence of $Ser^{189}$ stabilized TBK1 binding to TICAM-1 (Fig. 1*C*). Thus, the NTD may act as a repression domain within TICAM-1. Remarkably, exogenous NTD did not affect activation of IRF-3 or NF-κB by wild-type TICAM-1, the Δ180 mutant, or by TLR3-TICAM-1 activated with poly(I-C) (supplemental Fig. 1). We propose that exogenous NTD failed to interact with naive TICAM-1 because the TIR domain was occupied intramolecularly with NTD. Once TICAM-1 was recruited to TLR3, and oligomerized, the TRAF2/6 and TBK1 association sites appeared and signaling occurred quickly. When expressed with mutant Δ180, exogenous NTD interacted with the TIR domain of Δ180, whose binding site is distant from the TBK1 association sites, and did not affect TBK1 recruitment.

RIP1 binding to the C-terminal RHIM domain is necessary for TICAM-1 to mediate NF-κB activation (18), and the L194A mutant recruited RIP1 and activated NF-κB (Fig. 3*B* and supplemental Fig. 2). How NF-κB activation is controlled when TICAM-1 is in the resting form is unknown, but we surmise that the RHIM domain is unexposed in the resting state and that homodimerization opens the RHIM domain for RIP1 binding. $Pro^{434}$ in the BB loop of the TICAM-1-TIR domain is critical for TICAM-1 homodimerization, but the C-terminal homodimerization determinant remains unidentified (15). Further analysis is required to elucidate the mechanism of TICAM-1 activation.

TICAM-1 acts as a platform that accumulates signaling molecules to the TICAM-1 signalosome and triggers diversified cellular responses. TICAM-1-dependent gene expression directs mDCs to activate natural killer cells and cytotoxic T lymphocytes, which are both the most effective for antiviral response, and are an anti-cancer immune response (8, 9). Indeed, TLR3/4 ligands are strong candidates for adjuvant anti-cancer and infectious disease immunotherapy (10, 27–29). Interestingly, the RIG-I-like receptor-mediated signaling pathway shares most of its downstream signaling molecules with the TICAM-1 pathway, but it plays a distinct role in antivirus immunity by producing type I IFNs (30). Although TICAM-1-mediated signaling is initiated from the endosome, RIG-I-like receptor-mediated signaling occurs at the mitochondrial outer membrane (31). Hence, compartmentalization of signal platforms might be significant for activating distinct transcription factors, resulting in different cellular responses.

In certain RNA viral infections, TLR3-TICAM-1-dependent inflammatory cytokine and chemokine production affects virally induced pathology and host survival (32). In addition, biased activation of the TLR4-TICAM-1 pathway in lung macrophages by oxidized phospholipids triggers acute lung injury through cytokine production (11). Therefore, control of TICAM-1 activation is a novel therapeutic target for acute lung

injury. The development of an inhibitory molecule that blocks homo-oligomerization of TICAM-1 might be a straightforward approach for controlling excessive activation of TICAM-1 after viral infection.

*Acknowledgments—We are grateful to M. Sasai, K. Funami, A. Watanabe, H. Takaki, H. Shime, and T. Ebihara for invaluable discussions. Thanks are also due to T. Taniguchi (University of Tokyo) and M. Nakanishi (Nagoya City University, Nagoya, Japan) for providing the plasmids, and K. Arimoto (Kyoto University, Kyoto, Japan) and K. Shimotohno (Chiba Institute of Technology, Chiba, Japan) for providing reagents.*

## REFERENCES

1. Akira, S., Uematsu, S., and Takeuchi, O. (2006) *Cell* **124,** 783–801
2. Baccala, R., Hoebe, K., Kono, D. H., Beutler, B., and Theofilopoulos, A. N. (2007) *Nat. Med.* **13,** 543–551
3. O'Neill, L. A., and Bowie, A. G. (2007) *Nat. Rev. Immunol.* **7,** 353–364
4. Oshiumi, H., Matsumoto, M., Funami, K., Akazawa, T., and Seya, T. (2003) *Nat. Immunol.* **4,** 161–167
5. Yamamoto, M., Sato, S., Hemmi, H., Hoshino, K., Kaisho, T., Sanjo, H., Takeuchi, O., Sugiyama, M., Okabe, M., Takeda, K., and Akira, S. (2003) *Science* **301,** 640–643
6. Fitzgerald, K. A., Rowe, D. C., Barnes, B. J., Caffrey, D. R., Visintin, A., Latz, E., Monks, B., Pitha, P. M., and Golenbock, D. T. (2003) *J. Exp. Med.* **198,** 1043–1055
7. Oshiumi, H., Sasai, M., Shida, K., Fujita, T., Matsumoto, M., and Seya, T. (2003) *J. Biol. Chem.* **278,** 49751–49762
8. Schulz, O., Diebold, S. S., Chen, M., Näslund, T. I., Nolte, M. A., Alexopoulou, L., Azuma, Y. T., Flavell, R. A., Liljeström, P., Reis, e., and Sousa, C. R. (2005) *Nature* **433,** 887–892
9. Akazawa, T., Ebihara, T., Okuno, M., Okuda, Y., Shingai, M., Tsujimura, K., Takahashi, T., Ikawa, M., Okabe, M., Inoue, N., Okamoto-Tanaka, M., Ishizaki, H., Miyoshi, J., Matsumoto, M., and Seya, T. (2007) *Proc. Natl. Acad. Sci. U.S.A.* **104,** 252–257
10. Mata-Haro, V., Cekic, C., Martin, M., Chilton, P. M., Casella, C. R., and Mitchell, T. C. (2007) *Science* **316,** 628–632
11. Imai, Y., Kuba, K., Neely, G. G., Yaghubian-Malhami, R., Perkmann, T., van Loo, G., Ermolaeva, M., Veldhuizen, R., Leung, Y. H., Wang, H., Liu, H., Sun, Y., Pasparakis, M., Kopf, M., Mech, C., Bavari, S., Peiris, J. S., Slutsky, A. S., Akira, S., Hultqvist, M., Holmdahl, R., Nicholls, J., Jiang, C., Binder, C. J., and Penninger, J. M. (2008) *Cell* **133,** 235–249
12. Funami, K., Sasai, M., Ohba, Y., Oshiumi, H., Seya, T., and Matsumoto, M. (2007) *J. Immunol.* **179,** 6867–6872
13. Matsumoto, M., Funami, K., Tanabe, M., Oshiumi, H., Shingai, M., Seto, Y., Yamamoto, A., and Seya, T. (2003) *J. Immunol.* **171,** 3154–3162
14. Kagan, J. C., Su, T., Horng, T., Chow, A., Akira, S., and Medzhitov, R. (2008) *Nat. Immunol.* **9,** 361–368
15. Funami, K., Sasai, M., Oshiumi, H., Seya, T., and Matsumoto, M. (2008) *J. Biol. Chem.* **283,** 18283–18291
16. Sato, S., Sugiyama, M., Yamamoto, M., Watanabe, Y., Kawai, T., Takeda, K., and Akira, S. (2003) *J. Immunol.* **171,** 4304–4310
17. Fitzgerald, K. A., McWhirter, S. M., Faia, K. L., Rowe, D. C., Latz, E., Golenbock, D. T., Coyle, A. J., Liao, S. M., and Maniatis, T. (2003) *Nat. Immunol.* **4,** 491–496
18. Sharma, S., tenOever, B. R., Grandvaux, N., Zhou, G. P., Lin, R., and Hiscott, J. (2003) *Science* **300,** 1148–1151
19. Meylan, E., Burns, K., Hofmann, K., Blancheteau, V., Martinon, F., Kelliher, M., and Tschopp, J. (2004) *Nat. Immunol.* **5,** 503–507
20. Kaiser, W. J., and Offermann, M. K. (2005) *J. Immunol.* **174,** 4942–4952
21. Sasai, M., Oshiumi, H., Matsumoto, M., Inoue, N., Fujita, F., Nakanishi, M., and Seya, T. (2005) *J. Immunol.* **174,** 27–30
22. Häcker, H., Redecke, V., Blagoev, B., Kratchmarova, I., Hsu, L. C., Wang, G. G., Kamps, M. P., Raz, E., Wagner, H., Häcker, G., Mann, M., and Karin, M. (2006) *Nature* **439,** 204–207
23. Oganesyan, G., Saha, S. K., Guo, B., He, J. Q., Shahangian, A., Zarnegar, B., Perry, A., and Cheng, G. (2006) *Nature* **439,** 208–211
24. Horiuchi, M., Sakakibara, H., Kumeta, H., Takahashi, K., Enokizono, A., Ishii, A., Matsumoto, M., Seya, T., and Inagaki, F. (2008) *Biochem. Mol. Biol. Abstr.* 533,
25. Honda, K., and Taniguchi, T. (2006) *Nat. Rev. Immunol.* **6,** 644–658
26. Sasai, M., Tatematsu, M., Oshiumi, H., Funami, K., Matsumoto, M., Hatakeyama, S., and Seya, T. (2010) *Mol. Immunol.* **47,** 1283–1291
27. Salem, M. L., Kadima, A. N., Cole, D. J., and Gillanders, W. E. (2005) *J. Immunother.* **28,** 220–228
28. Seya, T., and Matsumoto, M. (2009) *Cancer Immunol. Immunother.* **58,** 1175–1184
29. Longhi, M. P., Trumpfheller, C., Idoyaga, J., Caskey, M., Matos, I., Kluger, C., Salazar, A. M., Colonna, M., and Steinman, R. M. (2009) *J. Exp. Med.* **206,** 1589–1602
30. Yoneyama, M., and Fujita, T. (2009) *Immunol. Rev.* **227,** 54–65
31. Seth, R. B., Sun, L., Ea, C. K., and Chen, Z. J. (2005) *Cell* **122,** 669–682
32. Matsumoto, M., and Seya, T. (2008) *Adv. Drug Deliv. Rev.* **60,** 805–812
33. Funami, K., Matsumoto, M., Oshiumi, H., Akazawa, T., Yamamoto, A., and Seya, T. (2004) *Int. Immunol.* **16,** 1143–1154
34. Iwamura, T., Yoneyama, M., Yamaguchi, K., Suhara, W., Mori, W., Shiota, K., Okabe, Y., Namiki, H., and Fujita, T. (2001) *Genes Cells* **6,** 375–388

AQ: C

AQ: B

**Identification of INAM, a polyI:C-inducible membrane protein, that participates in dendritic cell-mediated natural killer cell activation**

Takashi Ebihara[1,4,5], Masahiro Azuma[1,5], Hiroyuki Oshiumi[1], Kazuya Iwabuchi[2], Tadatsugu Taniguchi[3], Misako Matsumoto[1], and Tsukasa Seya[1]

[1]Department of Microbiology and Immunology, Hokkaido University Graduate School of Medicine, Kita-15, Nishi-7, Kita-ku, Sapporo 060-8638, Japan
[2]Division of Immunobiology, Institute for Genetic Medicine, Hokkaido University, Sapporo, Japan, 060-0815, Japan
[3]Department of Immunology, Graduate School of Medicine and Faculty of Medicine, University of Tokyo, Hongo 7-3-1, Bunkyo-ku, Tokyo, Japan

[4]Present address: Howard Hughes Medical Institute, Washington University School of Medicine, St. Louis, MO 63110

[5]Equally contributed authors



Running title: **INAM regulates NK activation**

Address correspondence to: Tsukasa Seya, Department of Microbiology and Immunology, Graduate School of Medicine, Hokkaido University, Kita-ku, Sapporo, 060-8638, Japan. Tel: 81-11-706-5073; FAX: 81-11-706-7866; E-mail: seya-tu@pop.med.hokudai.ac.jp

Key words: NK cell activation, dendritic cell, TLR3, TICAM-1 (TRIF), interferon regulatory factor 3 (IRF-3)

Total character count: 29,245



**SUMMARY**

In dendritic cells (mDC), TLR3 is expressed in the endosomal membrane and interacts with the adaptor TICAM-1 (TRIF). Stimulation of mDC TLR3 with polyI:C results in natural killer (NK) cell activation. This activation is triggered by mDC-NK contact but not cytokines. Using expression profiling to find genes with differential expression in polyI:C-stimulated TICAM-1-/- compared to wild mDC and lentiviral gain/loss-of-function analyses of mDC genes, we identified a TICAM-1-inducing membrane protein that participates in mDC-mediated NK activation based on augmentation of target cytotoxicity and IFN-γ production. Of the nine candidates screened, one contained a tetraspanin-like sequence. We have named the protein INAM, for IRF-3-derived NK-activating molecule, and found that INAM functioned in both mDC- and NK-sides to facilitate NK activation by mDC. Using knockout mDC and mice, TICAM-1, IPS-1 and IRF-3, but not IRF-7, were found to participate in mDC-mediated NK activation. The cytoplasmic tail of INAM participates in NK activation signal in NK cells. *In vivo*, adoptive transfer of INAM-expressing mDCs, but not lentivector control mDCs, into mice implanted with NK-sensitive tumors caused NK-mediated tumor regression. This report identifies a new pathway for mDC-NK contact-mediated NK activation that is governed by a TLR signal-derived membrane molecule.

## INTRODUCTION

Natural killer (NK) cells contribute to innate immune responses by killing virus-infected or malignantly transformed cells, and by producing cytokines such as IFN-γ and TNF-α. NK cell activation is determined by a balance of signals from inhibitory and activating receptors. Since ligands of inhibitory receptors include MHC class I and class I-like molecules, the absence of self-MHC expression leads to NK activation (1). Approximately twenty receptors contribute to NK activation (1, 2). When ligands for activating receptors are sufficient abundant, activating signals overcome inhibitory signals.

There are two currently accepted models for *in vivo* NK activation. One is that NK cells usually circulate in a "naïve" state, and are activated through interaction directly with ligands for pattern-recognition receptors (PRRs) expressed by NK cells, or interaction with cells that express PRR ligands (3, 4). When pathogens enter the host, innate immune sensors such as the Toll-like receptors (TLRs), RIG-I-like receptors, NOD-like receptors and lectin family proteins, which are PRRs, recognize a variety of microbial patterns (PAMPs) (5). Murine NK cells express almost all TLRs (TLR1-3, 4 and 6-9), and some of these are directly activated by pathogens with the help of IL-12, IL-18, IFN-γ and other cytokines (6). The other is that naïve NK cells tend to be recruited to the draining lymph nodes, where they are primed to be effectors with the help of mature myeloid dendritic cells (mDC), and released into peripheral tissues (7). mDC provide direct activating signals to NK cells through cell-cell contact (8-10). mDC also produce proinflammatory cytokines and IFN-α after recognizing PAMPs (6). In this case, however, the molecules and mechanisms in mDC that are dedicated to NK activation *in vivo* remain to be understood.

In this study, we focused on the molecules that are induced on mDC during maturation by exposure to double-stranded (ds) RNA, and the molecules involved in priming NK cells for target killing (8). dsRNA of viral origin and the synthetic analog polyI:C induce NK activation in concert with mDC *in vivo* and *in vitro* (11). PolyI:C is recognized by the cytoplasmic proteins RIG-I/MDA5 and the membrane protein TLR3, both of which are expressed in mDC (12). When RIG-I and MDA5 in the cytoplasm deliver a signal to the adaptor protein, Interferon promoter stimulator-1 (IPS-1, also known as MAVS, VISA, and Cardif) on the mitochondria outer membrane (13-16), TLR3 in the endosomal membrane recruits the adaptor protein, TICAM-1/TRIF (17, 18). Both adaptor proteins activate TBK1 and/or IKKε, which phosphorylate IRF-3 and IRF-7 to induce type I interferon (IFN) (19). We previously showed that the TLR3/TICAM-1 pathway in mDC participates in inducing anti-tumor NK cytotoxicity by polyI:C (8). mDC matured with polyI:C can enhance NK cytotoxicity through





mDC-NK cell/cell contact (8). Therefore, we hypothesized that an unidentified protein is up-regulated on the cell surface of mDC through activation of the TLR3/TICAM-1 pathway, and this protein enables mDC to interact with, and activate NK cells. This is the first report identifying an IRF-3-derived NK-activating molecule, which we named INAM. INAM is a TICAM-1-inducible molecule on the cell surface of bone marrow-derived dendritic cells (BMDC) that activates NK cells via cell-cell contact. Our data imply that mDC harbor a pathway for NK activation that acts in conjunction with dsRNA and TLR3.

## RESULTS

### TICAM-1/IRF3 signal in BMDCs augments NK activation

An *in vitro* system for evaluating NK activation through BMDC-NK contact was established for this study (Fig. 1A). A mouse melanoma cell subline B16D8, which was established in our lab as a low H-2 expressor (20), was used as an NK target. PolyI:C, wild-type (WT) BMDC and NK cells were all found to be essential for NK-mediated B16D8 cytolysis in the *in vitro* assay (Fig. 1A). PolyI:C-mediated NK activation was at baseline levels in a transwell with a 0.4 μm pore, suggesting the importance of direct BMDC-NK contact for this cytolysis induction (Fig. 1A). When wild-type BMDC were replaced with TICAM-1-/- BMDC in this system, polyI:C-mediated NK activation was partly abolished (Fig. 1B, Fig. S1). TICAM-1 of BMDC, but not of NK cells, was involved in driving NK activation, and ultimately B16D8 cells were damaged by BMDC-derived NK cells (Fig. 1B). PolyI:C-mediated NK activation occurred even when WT NK cells were replaced with TICAM-1-/- NK cells (Fig. 1B), which means that NK activation barely depends on the TICAM-1 pathway in NK cells.

Intraperitoneally injected polyI:C activated splenic NK cells in B6 mice to kill B16D8 cells *ex vivo,* consistent with previous reports (21, 22), and this polyI:C-mediated NK activation was markedly reduced in IPS-1-/- mice established in our lab (Fig. S1C), suggesting that NK cell activation is induced via not only the TICAM-1 pathway but also the IPS-1 pathway, which was largely comparable with previous reports (21, 22). IPS-1 in BMDC was more involved in polyI:C-driven NK cytotoxicity than TICAM-1 but almost equally contributed to NK-dependent IFN-γ induction to TICAM-1 in our setting (Fig. S1B). In addition, the serum level of IL-12p40 in polyI:C-treated mice was largely dependent on TICAM-1 (Fig. S1D) (8,23). These results suggest that polyI:C activates NK cells not directly but secondary to mDC maturation, which is sustained by the IPS-1 or TICAM-1 pathway of mDC. Even though NK cells express TLR3, they are only minimally activated by polyI:C alone. Signaling by TICAM-1 in BMDC can augment NK cytotoxicity and IFN-γ production

via BMDC/NK contact.

The TICAM-1 pathway activates the transcription factors IRF-3. More precisely, exogenous addition of polyI:C can activate endosomal TLR3 and cytoplasmic RIG-I/MDA5. RIG-I/MDA5 assembles the adaptor IPS-1 which in turn recruits the NAP1/IKKε/TBK1 kinase complex and activates both IRF-3 and IRF-7 (24, 25). For this reason, we examined the role of IRF-3 and IRF-7 in BMDC for activation of NK cells by polyI:C. Activation of IRF-3 but not IRF-7 was required for BMDC to induce NK cytotoxicity (Fig. 1C). IL-2 (26), IFN-α (10) and trans-presenting IL-15 (9) induced by BMDC are reported to be key cytokines for BMDC -mediated NK activation in response to polyI:C. However, even with normal levels of IFN-α production and IL-15 expression (Fig. 1D and 1E), TICAM-1-/- BMDC failed to induce full NK cytotoxicity (Fig. 1B). In contrast, IRF-7-/- BMDCs, which have impaired IFN-α and IL-15 expression, fully activated NK cells (Fig. 1C, 1D and 1E). Hence, in BDMCs, the TICAM-1/IRF-3 pathway, rather than other cytokines, appears to induce cell-surface molecules that mediate BMDC/NK contact and evoke NK cytotoxicity.

**Identification of INAM**

To identify the NK-activating cell surface molecule on BMDC, we performed microarray analysis on polyI:C-stimulated BMDC prepared from TICAM-1-/- and WT mice. The results yielded nine TICAM-1-inducible molecules with transmembrane motifs. Six were induced in an IRF-3-dependent manner, while three were still induced in IRF-3-/- BMDC. The NK-activating ability of the products of these genes was investigated by introduction of lentivirus expression vector into IRF-3-/- BMDC. BMDC having the transduced genes were co-cultured with wild-type NK cells and polyI:C, and the NK-activating abilty evaluated by determining IFN-γ in the 24 h co-culture. NK cells, but not the gene-transduced BMDC, produced IFN-γ in the presence of polyI:C. Finally, we identified a tetraspanin-like molecule that satisfied our evaluation criteria (IFN-γ and cytotoxicity) on the mDC-NK activation, and named this molecule INAM. INAM clearly differed from other tetraspanins like CD9, CD63, CD81, CD82 and CD151 in the predicted structure. Murine INAM is a 40-55 kDa protein with one N-glycosylation site and possesses four transmembrane motifs (Fig. 2A and 2B). Western blotting analysis of INAM-transfected cells under nonreducing conditions showed no evidence of multimers (Fig. 2B). The N-terminal and C-terminal regions of INAM are in the cytoplasm, since anti-Flag antibody did not detect C-terminal Flag-tagged INAM until cells were permeabilized (data not shown).

Alignment of the predicted amino acid sequence of mouse INAM with thatof the human ortholog revealed that the two INAMs shared 71.7% a.a. identity. INAM is also



called FAM26F, and is in the FAM26 gene family (27, 28). Sequence database searches identified six mouse INAM paralogs. While FAM26A/CALHM3, FAM26B/CALHM2 and FAM26C/CALHM1 are located on chromosome 19, FAM26D, FAM26E and FAM26F/INAM are on chromosome 10. Only INAM was inducible with TLR agonists (data not shown). All FAM26 family proteins have three or four transmembrane motifs predicted by the TMHMM Server ver.2.0. Human CALHM1 has a conserved region (Q/R/N site) with ion channel properties at the C-terminal end of the second transmembrane motif that controls cytoplasmic $Ca2^+$ levels (28). However, the Q/R/N site was not found in INAM. CALHM1, 2 and 3 are highly expressed in brain. Quantitative RT-PCR revealed that INAM expression was high in spleen and lymph nodes (LN) while low in thymus, liver, lung and small intestine (Fig. 2C), although expression of the other two FAM26 family members from chromosome 10 was highest in brain (data not shown). All splenocytes examined ($CD3^+$, $CD19^+$, $DX5^+$, $CD11b^+$, $CD11c^+$, mDCs: $CD11c^+PDCA1^-$, pDCs: $CD11c^-PDCA1^+$) expressed INAM to some levels (Fig. 2D). The INAM expression was inducible by polyI:C in LN cells (Fig. 2E): the induction levels were more prominent in myeloid cells than in lymphocytes in the lymph nodes (Fig. S2A). $NKp46^+$ and $DX5^+$ NK cells also expressed INAM with low levels and the levels were slightly increased by polyI:C stimulation (data not shown). Notably, only $CD45^+$ cells expressed INAM, which excludes the participation of contaminating stromal cells in the INAM up-regulation (Fig. S2B).

**BMDC INAM activates NK cells**

WT and IRF-7-/- BMDC induced high NK cytotoxicity in response to polyI:C while TICAM-1-/-, IPS-1-/- and IRF-3-/- BMDC showed less NK activation (Fig. 1B, 1C and Fig. S1). INAM-expression profile by polyI:C stimulation was then examined using WT, IRF-3-/-, IRF-7-/- and TICAM-1-/- BMDC. Stimulation with polyI:C induced INAM with normal level in IRF-7-/- BMDC but at decreased levels in IRF-3-/- and TICAM-1-/- BMDC (Fig. 3A). The expression profiles of INAM in polyI:C-stimulated BMDC were in parallel with those inducing NK activation. BMDC express a variety of TLRs (29) but other TLR ligands, $Pam_3CSK_4$ for TLR1/2, Malp2 for TLR2/6, and CpG for TLR9, barely induced INAM on BMDC. High induction of INAM was observed in BMDC stimulated with LPS as well as polyI:C (Fig. 3B), both of which can activate TICAM-1 to induce IRF-3 and IFN-α activation (17, 18, 24, 30, 31). Since INAM is an IFN-inducible gene (Fig. 3B), INAM induction may by amplified by type I IFNs.

We next examined whether INAM was localized to the cell surface membrane in BMDC. Immunofluorescence analysis showed Flag-tagged-INAM on the cell surface of

BMDC. Plasma membrane expression of INAM was also confirmed by cell surface biotinylation (Fig. S3). Although the lentivirus infection was not very efficient toward BMDC, GFP-expression levels were similar in cells with control virus and those with INAM-expressing virus (Fig. 3C). Transduction efficiency and expression from the lentivirus vector were adjusted using GFP expression (Fig. S4), and surface INAM expression was further confirmed with BMDC, NK cells and INAM-expressing BaF3 (INAM/BaF3) cells, in some case using polyclonal Ab against INAM (Fig. S5).

We then examined whether overexpressing INAM resulted in signaling that directed BMDC maturation and production of cytokines, including IFN-α and IL-12p40, which are reported to enhance NK activity (3, 9, 10). The status of INAM-transduced BMDC was assessed by CD86 expression and cytokine production, and no significant differences in these maturation markers were seen in BMDC overexpressing INAM (Fig. S6). In addition, polyI:C-mediated NK activation occurred in BMDC expressing an INAM mutant lacking the cytoplasmic C-terminal region (193-327aa) (Fig. 4A,B), excluding the participation of the cytoplasmic region in BMDC mature signaling.

To investigate whether INAM could reconstitute NK-activating ability in IRF-3-/- BMDC, we transduced INAM into IRF-3-/- BMDC. Overexpression of INAM in IRF-3-/- BMDC induced NK IFN-γ production and NK cytotoxicity against B16D8, and this NK activation was further enhanced by the addition of polyI:C (Fig. 3D and 3E). Thus, polyI:C may also work for NK activation. Direct cell-cell contact with NK cells was required for INAM on BMDC to augment NK activity (Fig. 3F). We silenced the INAM gene in BMDC using the lentiviral vector pLenti-dest-IRES-hrGFP, and monitored expression by GFP. Since transfection efficiency was relatively high in this case compared to that shown in Fig. 3C, the expression level of INAM had decreased by ~75% in wild-type BMDC compared to the non-silenced control (Fig. 3G, Fig. S7A). PolyI:C response of BMDC-inducible cytokines tested was not altered by INAM silencing in BMDC (Fig. S7B). Yet, this INAM RNA interference caused a significant decrease in NK cell IFN-γ production after co-culture of the INAM-knockdown BMDCs and WT NK cells with polyI:C (Fig. 3H). Taken together, these results indicate that INAM is downstream of IRF3 in BMDC and involved in the activation of NK cells by BMDC.

Using INAM-expressing stable BaF3 cell line (INAM/BaF3), we tested the possibility that INAM is an activating ligand for NK cells. As a positive control, we produced a stable BaF3 cell line expressing Rae-1α (Fig. S8A) which is a ligand for the NK-activating receptor NKG2D (32). Although Rae-1α/BaF3 cells were easily damaged by IL-2-activated NK cells, INAM/BaF3 cells were not (Fig. S8B). In this context, addition of IRF-3-/- BMDC to this culture with BaF3 and NK cells led to slight



augmentation of IFN-γ induction irrespective of the presence of INAM on BaF3 cells (Fig. S8C), and β2-microglobulin -/- BMDC barely affected the IFN-γ level (data not shown). These results suggest that an INAM-containing molecular matrix, rather than INAM alone, acts toward NK cells. Alternatively, INAM may selectively function with specific mDC molecules to activate NK cells.

**INAM on NK cells is required for efficient NK activation**

mDC were previously shown to be required for efficient NK activation *in vivo* and *in vitro* (8). We found that INAM was present in BMDC and NK cells and polyI:C acts on both side (Figs. 2D, 3D, and 3E). Tetraspanin-like molecules tend to work as scaffolds for heteromolecular complexes that contain molecules functioning in a cis- or trans-adhesion manner to exert intercellular or extracellular functions. Thus, the function of INAM may not be confined to mDC, so we studied the function of INAM on NK cells. In NK cells, INAM was also inducible by polyI:C (Fig. 5A, Fig. S2A), and the induction of INAM was abrogated completely in IRF-3-/- NK cells, and moderately in TICAM1-/- NK cells (Fig. 5B). This suggests that polyI:C acts on NK cells also, and induces INAM through IPS-1/IRF-3 activation when NK cells are co-cultured with BMDC and polyI:C.

To investigate whether INAM induced in NK cells is associated with BMDC-mediated NK activation, we stimulated INAM-transduced IRF-3-/- BMDC with polyI:C for 4 h, washed polyI:C out and cultured the cells with WT NK cells. Under these conditions, in which polyI:C acted not on NK cells but only on BMDC, little NK activation was observed (Fig. 5C). Furthermore, IRF-3-/- NK cells produced little IFN-γ when co-cultured with WT BMDC and polyI:C (Fig. 5D). INAM-overexpressing IRF-3-/- BMDC required IRF-3 in NK cells for efficient BMDC-mediated production of IFN-γ from NK cells (Fig. 5D). We next transduced INAM into IRF-3-/- NK cells using a lentivirus (INAM/pLenti-IRES-hrGFP) to reconstitute NK IFN- γ-producing activity. IRF-3-/- NK cells were transfected with INAM-expressing lentiviral vector, and cultured for 3 days with high concentrations of IL-2 (500 IU/mL). Transfection efficiency was assessed by GFP expression (Fig. 5E), and the NK cells were co-cultured with wild-type BMDC. The IRF-3-/- NK cells with INAM expression secreted IFN-γ at significantly higher levels than controls, in the presence of wild-type BMDC (Fig. 5F). These data indicate that INAM is induced by polyI:C through IRF-3 activation, not only in BMDC, but also in NK cells, and that INAM on NK cells synergistically works with INAM on BMDC for efficient NK activation. Both INAMs on BMDC and NK cells are essential for BMDC-mediated NK activation.

We next checked the function of the C-terminal stretch of INAM in NK activation.

Although intact INAM works in NK cells to produce IFN- γ in response to BMDC (Fig. 5F), introduction of C-del INAM into IRF3-/- NK cells did not result in high induction of IFN-γ in response to BMDC (Fig. 4C). Thus, INAM participates in NK activation through its cytoplasmic regions, which has no significant role in BMDC for NK activation.

**Antitumor NK activation via INAM-expressing BMDCs *in vivo***

mDC-mediated NK activation induces antitumor NK cells, which cause regression of NK-sensitive tumors (8, 33). We tested the *in vivo* function of INAM-expressing BMDC using B16D8 tumor-bearing mice. BMDC were used 24 h after transfection with either INAM/pLenti-IRES-hrGFP or control pLenti-IRES-hrGFP, and injected twice a week subcutaneously around a pre-existing tumor in tumor-implanted mice, beginning 11-13d after tumor challenge. INAM-expressing BMDC significantly retarded tumor growth (Fig. 6A). Tumor retardation was abrogated by depletion of NK1.1-positive cells (Fig. 6B). Thus, INAM expression on BMDC contributed to anti-tumor NK activation *in vivo*.

When the control or INAM-expressing IRF-3-/- BMDC were co-cultured with WT NK cells *in vitro*, there was no induction of the mRNA of TRAIL and Granzyme B in NK cells (Fig. 7A). TRAIL and Granzyme B were induced in NK cells by the addition of polyI:C to the mixture, and INAM expression in BMDC up-regulated mRNA levels of TRAIL and Granzyme B (Fig. 7A). *In vivo* administration studies were performed with polyI:C-treated WT BMDC or INAM-expressing IRF-3-/- BMDC to test their ability to up-regulate the mRNA levels of TRAIL and Granzyme B in NK cells in draining LN (Fig. 7B). INAM-expressing IRF-3-/- BMDC showed comparable abilities to up-regulate the killing effectors with polyI:C-treated BMDC (Fig. 7B). Taken together, INAM has therapeutic potential for NK-sensitive tumors by activating NK cells.

**DISCUSSION**

Previous reports demonstrated that mDC/NK interaction leads to direct NK activation and damages NK target cells *in vitro* (3, 8-10). In addition, mDC initiate NK cell-mediated innate antitumor immune responses *in vivo* (8, 33, 34). Systemic administration of polyI:C unequivocally results in activation of peripheral NK cells (3, 8, 35). Although the molecular mechanism by which mDC prime NK cells was still unclear, the TICAM-1 pathway and IPS-1 pathway have been reported to participate in polyI:C-mediated mDC maturation that drives NK-activation (8, 21, 22). We have shown in an earlier study that mDC disrupted in the TLR3-TICAM-1 pathway abrogate



NK cell activation (8, 34). In TICAM-1-/- mice, NK-sensitive implant tumors grew well as those in wild-type mice depleted of NK cells (8). mDC gain high antitumor potential against B16D8 implant tumors through lentiviral transfer of TICAM-1, which is attributable to NK activation (8). We further showed that TICAM-1 is a critical molecule for mDC to induce NK cell IFN-γ as well as IPS-1 and participates in driving NK cytotoxicity to a lesser extent than IPS-1. Here, we clarified a molecular mechanism by which mDC immediately promote NK cell functions *in vitro* and *in vivo*.

Our findings showed that IRF-3 is the transcription factor that is downstream of TICAM-1 responsible for maturing mDC to an NK-activating phenotype. We discovered that INAM, a membrane-associated protein, is up-regulated on the surface of mDC by polyI:C stimulation, and activates NK cells via cell-cell contact. Furthermore, we found that NK cells also express INAM on their cell surface after polyI:C stimulation. mDC-NK activation by polyI:C can be reproduced with INAM-transduced mDC and NK cells, and adoptive transfer experiments show that INAM-overexpressing mDC may have therapeutic potential against B16 melanoma cells in an NK-dependent manner. These functional properties of INAM-expressing mDC fit the model of mDC priming NK activation. Ultimately, INAM appears to be the key molecule in the previously reported mechanism of mDC-NK contact activation.

After the submission of this manuscript, two papers were published where the MDA5/IPS-1 pathway in mDC is more important for driving NK activation (21,22). Our data also support this point using the IPS-1-/- mice we established. However, it remains to be settled whether TICAM-1 and IPS-1 take the same INAM complex as a common NK activator in mature mDC, and whether TLR3 (or MDA5) KO is equivalent to TICAM-1 (or IPS-1) KO in the mDC-NK activation model.

PolyI:C activates IRF-3 through the two pathways involving the adaptors IPS-1 and TICAM-1 (12, 23, 25). The two pathways share the complex of IRF-3-activating kinase, NAP1, IKKε and TBK1, that is downstream of adaptors (19). Nevertheless, these pathways are capable of inducing a number of genes unique to each adaptor. While IFN-α production by *in vivo* administration of polyI:C is largely dependent on the IPS-1 pathway, IL-12p40 is mainly produced by the TICAM-1 pathway (23). Therefore, it is not surprising that INAM induction is predominant in the TICAM-1 pathway in polyI:C-stimulated BMDC (Fig. 3A). What happens in IRF-7-/- BMDCs in terms of INAM induction and what mechanism sustains BMDC IPS-1-mediated activation of NK cells will be issues to be elucidated in the future.

Although IRF-3-regulated cell-surface INAMs are required for efficient interaction between BMDC and NK cells, the mechanism by which forced expression of INAM causes signaling for BMDC maturation is still unknown. Although the